THE PROPERTIES AND WELDABILITY OF LOW ACTIVATION FERRITIC STEELS

Bryan A. Chin
Annual Report
May 11, 1990

Grant #DE-FG05-86ER52139
Materials Engineering
Auburn University
Auburn, AL 36849

DOE/ER/52139--90-1

DE90 011872

THE PROPERTIES AND WELDABILITY OF LOW ACTIVATION FERRITIC STEELS

Bryan A. Chin
Annual Report
May 11, 1990

Grant #DE-FG05-86ER52139
Materials Engineering
Auburn University
Auburn, AL 36849

TABLE OF CONTENTS

LIST OF TABLES

LIST OF FIGURES

EXECUTIVE SUMMARY OF ACCOMPLISHMENTS

1. Weldability of Low Activation Ferritic Alloys

A comprehensive study of the microstructure and mechanical properties of the first generation of Low Activation Ferritic Alloys was completed. The results indicate that all alloys tested are weldable. However, several alloys were found to be susceptible to decarburization during heat treatment. Post-weld heat treatment is necessary in the 9-12 Cr steels to restore toughness.

2. Brazing of Copper-Alumina Alloys

An induction braze has been developed to join copper-alumina alloys. This brazing technique is proposed to replace current furnace brazing techniques that have yielded poor results because of silver ingression along the fine grain boundaries of copper-alumina alloys. The induction braze (because of the short braze time) severely restricts silver ingression along the grain boundaries of copper-alumina alloys. Tensile tests of induction brazed lap joints fail in the base material rather than the braze indicating good braze properties.

3. Welding of Helium Containing Stainless Steel

A method of welding stainless steel containing 105 and 256 appm helium has been found which appears to eliminate catastrophic cracking of the completed weld. Preliminary tests show that the growth and coalescence of helium grain boundary bubbles can be preferentially altered from grains oriented parallel to the weld direction to grains oriented perpendicular to the weld direction. Studies are underway to confirm the mechanisms responsible for helium bubble reorientation and the elimination of weld cracking.

WELDABILITY OF LOW ACTIVATION FERRITIC STEELS FOR FUSION REACTOR APPLICATIONS

Chin-An Wang

ABSTRACT

A series of ferritic steels patterned on the chromium-molybdenum alloys, 2 1/4Cr-1Mo, 9Cr-1MoVNb and 12Cr-1MoVW, were tested for weldability. These steels are being developed as candidates for the first wall and blanket structures of fusion reactors. Use of these materials will minimize the long term radioactive hazards associated with disposal after service. In these low activation alloys, elements which become activated during irradiation with long half lives (Mo and Nb) are replaced. The major changes include the replacement of molybdenum with tungsten, the addition of vanadium in 2 1/4% Cr steels, and the replacement of niobium in the 9% Cr steel with tantalum. These replacement elements radically modify both the mechanical properties and weldability of the alloys.

In this study, the effect of the alloy modifications on the microstructure and the mechanical properties of the welds are presented. Bainitic steels (2 1/4 Cr%) usually exhibit good weldability, while the martensitic steels (5, 9 and 12 Cr%) are suspectable to embrittlement in the heat affected zone (HAZ). The objective of this study was to characterize the welded microstructure and mechanical

properties of these low activation alloys. Autogenous bead-on-plate welds were produced using the gas tungsten arc welding (GTAW) process. Microstructure, microhardness, weld bend and tensile test results are reported for the base metal, heat affected zone and fusion zone of the weld.

I. INTRODUCTION

Considerable effort has been devoted to the development of fusion reactor systems during the past three decades. Nevertheless, the realization of an economical fusion reactor for electrical power generation is still not practical. This is due to the complex problems and difficulties inherent in plasma physics, engineering design, materials development and optimization of such a system.

Several fusion systems have been proposed and considered in power generation, namely magnetically-confined (tokamak and mirror), inertially-confined (laser and ion) and hybrid (fusion-fission) systems. The magnetically-confined tokamak reactor has been extensively studied since the 1960s. Tokamak is a Russian acronym which consists of the first syllables of the Russian words: toroid, kamera (chamber), magnit (magnet) and the first letter of the word katushka (coil). The tokamak concept is the most dominant fusion approach in the world and most probably, the first fusion reactor used in power generation will be of this type [1,2].

Although many fusion fuel cycles have been proposed, the principal reactions during the operation of a fusion

reactor include deuterium-deuterium (D-D), deuterium-tritium (D-T) and deuterium-^{3}He (D-^{3}He) as follows [2,3]:

$$^2D + {}^2D \rightarrow {}^3T\ (1.01\ MeV) + p\ (3.03\ MeV) \quad \text{------(1)}$$

$$^2D + {}^2D \rightarrow {}^3He\ (0.82\ MeV) + n\ (2.45\ MeV) \quad \text{------(2)}$$

$$^2D + {}^3T \rightarrow {}^4He\ (3.52\ MeV) + n\ (14.05\ MeV) \quad \text{------(3)}$$

$$^2D + {}^3He \rightarrow {}^4He\ (3.67\ MeV) + p\ (14.67\ MeV) \quad \text{------(4)}$$

In a tokamak fusion reactor, the first wall and blanket are the inner most structural components adjacent to the fusion plasma. The first wall structure surrounds the reaction plasma and acts as a vacuum chamber with a protective ceramic coating barrier on the surface facing the plasma. The blanket serves several functions. It slows down fast neutrons and provides reflectors to reflect scattered or leaking neutrons back into the reactor core. It also acts as a coolant container which carries the energy away as heat for electrical power generation and contains the tritium breeding materials so that the D-T reaction can be sustained.

The neutrons, derived from the above reactions, impinge on the components of the fusion reactor. The neutron flux decreases approximately exponentially with increasing distance from the plasma chamber. Therefore, the first wall and blanket will suffer the highest neutron flux compared to the other structural components and become highly

radioactive from activation by highly energetic neutrons, mainly from reaction (3), during operation [1-5]. A schematic of the tokamak D-D fusion reactor, WILDCAT, is shown in Figure 1 [6].

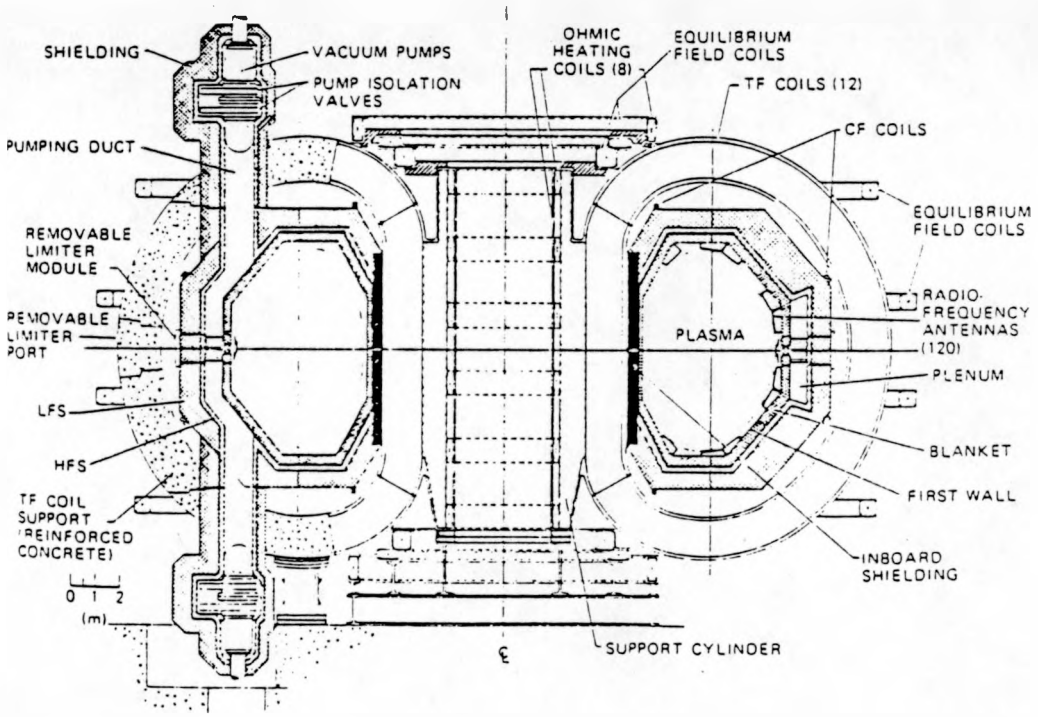

Figure 1. Cross Section of a Tokamak D-D Fusion Reactor, Wildcat.

Public safety and environmental contamination concerns arise from the long term radioactive hazards associated with disposal of these structural components after service. This concern led the Office of Fusion Energy of the U.S. Department of Energy to establish a program to develop low activation steels for fusion reactor applications in 1982 [6]. The objective of the program is to develop materials which will fall within Class C of the nuclear waste storage guidelines issued by the U.S. Nuclear Regulatory Commission (10 CFR part 61), but with the hope to meet Class B criteria [7]. The guidelines are shown in Table 1.

Several criteria have been proposed and discussed for the development of first wall and blanket materials. One of the requirements is sound joining. Welding is an important method to fabricate engineering alloys into structural components [1].

In this study, a series of ferritic steels patterned on the chromium-molybdenum alloys, 2 1/4 Cr-1Mo, 9 Cr-1MoVNb and 12 Cr-1MoVW, were tested for weldability. These steels are being developed as candidates for the first wall and blanket structures of fusion reactors. Use of these materials will minimize the radioactive impact on three areas: (1) disposal of radioactive waste, (2) reactor maintenance and (3) reactor safety.

In these alloys, elements which become activated during irradiation with long half lives (Mo, Nb and Co etc.) are

Table 1. Nuclear Waste Classification and Storage Under Proposed 10CFR61 Rules.

Waste class	Definition	Disposal
Class A - Segregated	Decays to acceptable levels during site occupancy	
Class B - Stable	Stabilized; decays within 100 years to levels that are not a danger to public health and safety	Covered to reduce surface radiation to a few percent of background
Class C - Intruder	Decays to acceptable safe levels in times greater than 100 years but less than 500 years	At least 5 M below the surface with natural or engineered barriers
Waste that does not meet Class C definition	Decay times greater than 500 years	Does not qualify for near-surface disposal; proposed methods will be considered on a case-by-case basis

replaced. Because W behaves like Mo in steels, it was proposed as a replacement for Mo. Since W has about twice the atomic weight of Mo, 2% W was used based on an atom-for-atom replacement [8]. The major changes include the replacement of molybdenum with tungsten, the addition of vanadium in 2 1/4% Cr steels, and the replacement of niobium in the 9% Cr steels with tantalum. These replacement elements radically modify both the mechanical properties and weldability of the alloys.

Bainitic steels (2 1/4% Cr) usually exhibit good weldability, while martensitic steels (5,9 and 12% Cr) are suspected to have inadequate toughness in the heat affected

zone (HAZ) due to the presence of untempered martensite [9]. The objective of this study was to characterize the welded microstructure and mechanical properties of these low activation steels. In order to explore the weldability of these steels, the structure and properties of autogenous bead-on-plate welds produced using the gas tungsten arc welding (GTAW) process was evaluated. Microhardness, weld bend and tensile test results are reported for the base metal, heat affected zone and fusion zone of the weld.

II. LITERATURE REVIEW

Welding Metallurgy

Welding is the most effective and important method of joining and fabricating materials into structural components. Several metallurgical phenomena are involved during the welding operation, such as melting, solidification, gas-metal reaction, surface phenomena, and solid state reaction, etc. The major difference with respect to the general metallurgical field is that the reactions occur very rapidly during welding. In this study, eight heats of newly developed low activation ferritic steels were examined for weldability. The chemical compositions of these steels are given in Table 2.

It is generally found that the microstructure in a gas tungsten arc weld consists of three distinct regions: fusion zone (FZ), heat-affected zone (HAZ) and base metal. The fusion zone weld metal and HAZ must be compatible with the base metal to be joined, if a successful joint is to be produced. When steels are joined by fusion welding, the material of the plates has to be heated to its melting point, where the fusion zone weld metal is formed, and then

Element	Chemical Composition, wt%								
	2¼Cr–¼V Heat 3785	2¼Cr–1W–¼V Heat 3786	2¼Cr–2W Heat 3787	2¼Cr–2W–¼V Heat 3788	5Cr–2W–¼V Heat 3789	9Cr–2W–¼V Heat 3790	9Cr–2W–¼V–Ta Heat 3791	12Cr–2W–¼V Heat 3792
C	0.11	0.10	0.11	0.11	0.13	0.12	0.10	0.10
Mn	0.40	0.34	0.39	0.42	0.47	0.51	0.43	0.46
P	0.015	0.015	0.016	0.016	0.015	0.014	0.015	0.014
S	0.006	0.006	0.005	0.006	0.005	0.005	0.005	0.005
Si	0.17	0.13	0.15	0.20	0.25	0.25	0.23	0.24
Ni	0.01	0.01	<0.01	<0.01				
Cr	2.36	2.30	2.48	2.42	5.00	8.73	8.72	11.49
Mo	0.01	<0.01	<0.01					
V	0.25	0.25	0.009	0.24	0.25	0.24	0.23	0.23
Nb	<0.01	<0.01	<0.01					
Ta	<0.01	<0.01	<0.01				0.075	
Ti	<0.01	<0.01	<0.01					
Co	0.005	0.006	0.008					
Cu	0.02	0.025	0.03					
Al	0.02	0.02	0.02	0.021	0.03	0.03	0.03	0.028
B	<0.001	<0.001	0.001					
W		0.03	1.99	1.98	2.07	2.09	2.09	2.12

[a] Balance iron.

Table 2. Chemical Compositions of Low Activation Ferritic Steels.

cooled again rapidly under restrained conditions imposed by the geometry of the joint. As a result of this, the original microstructure and properties of the metal in a region close to the weld are changed. This area of the weld is usually referred to as the heat-affected zone.

The heat-affected zone is conveniently divided into two sub-regions: grain-growth region and grain-refined region. The grain-growth region is adjacent to the weld interface and has experienced peak temperatures approaching the solidus of the base metal. Therefore, prior austenite grains grow and rapidly become coarse grains before transformation occurs. The grain-refined region is farther away from the weld interface and is brought into the lower temperature portion of the austenite region. Prior austenite grains do not have sufficient time to grow and remain very small [10].

Bainite Structure

Within the Time-Temperature-Transformation (TTT) diagram for a carbon steel, there is a wide range of temperature, usually 250 to 550°C, in which neither pearlite nor martensite forms. In this region, bainite which is composed of lath-shaped fine aggregates of ferrite and cementite is formed. Bainite possesses some of the properties of the phases produced by high temperature reactions involving ferrite and pearlite as well as some of the characteristics of phases produced by the martensite

reaction. Bainite also occurs during treatments at cooling rates too fast for pearlite to form, yet not rapid enough to produce martensite.

In plain carbon steels, the bainitic reaction is kinetically shielded by the ferrite and pearlite reactions which commence at higher temperature and short time, so that in continuously-cooled samples, a bainitic structure is difficult to obtain. The addition of metallic alloying elements usually results in retardation of the ferrite and pearlite reaction, and the bainite reaction is depressed to a lower temperature. This often leads to greater separation of the bainite reaction. The TTT curves for many alloy steels show much more clearly separate C-curves for the pearlite and bainite reactions [11,12]. Figure 2 shows continuous cooling C-curves for a steel containing 0.7%C, 0.36%Si, 0.84%Mn, 1.4%Ni and 0.47%Mn [13].

Bainite, a typical structure obtained in 2 1/4% Cr steel, can possess relatively high strength levels together with adequate ductility. The steels are readily weldable, because bainite rather then martensite will form in the heat-affected zone adjacent to the weld metal, and so the incidence of weld cracking is greatly reduced. Furthermore, the steels have low carbon content, which improves the weldability and reduces stresses arising from the transformations.

A very effective means of isolating the bainite reaction in low carbon steels has been found to be the addition of 0.002% soluble boron (B) to a 0.5% Mo steel. While the straight Mo steel encourages the bainite reaction, the boron markedly retards the ferrite reaction, probably by preferential segregation to the prior austenite boundaries [12,14,15]. Further control of the reaction is obtained by use of elements such as Ni, Cr, and Mn which depress the temperature of maximum rate of formation of bainite. As the transformation temperature is lowered, for a constant cooling rate, the strength of the steel increases substantially but is accompanied by a loss of ductility.

Martensite Structure

Martensite, generally found in high Cr (5, 9 and 12%) steels, is favored by a transformation under a very high cooling rate [8,9,17]. The critical rate of cooling required is very sensitive to the alloying elements present in the steel and, in general, will be lower for higher total alloy concentration. The cooling rate must be sufficient to suppress the higher temperature diffusion-controlled ferrite and pearlite reactions, as well as other intermediate reactions such as the formation of bainite.

The reaction begins at the martensite start temperature, M_s, which can vary over a wide temperature range from as high as 500°C to well below room temperature,

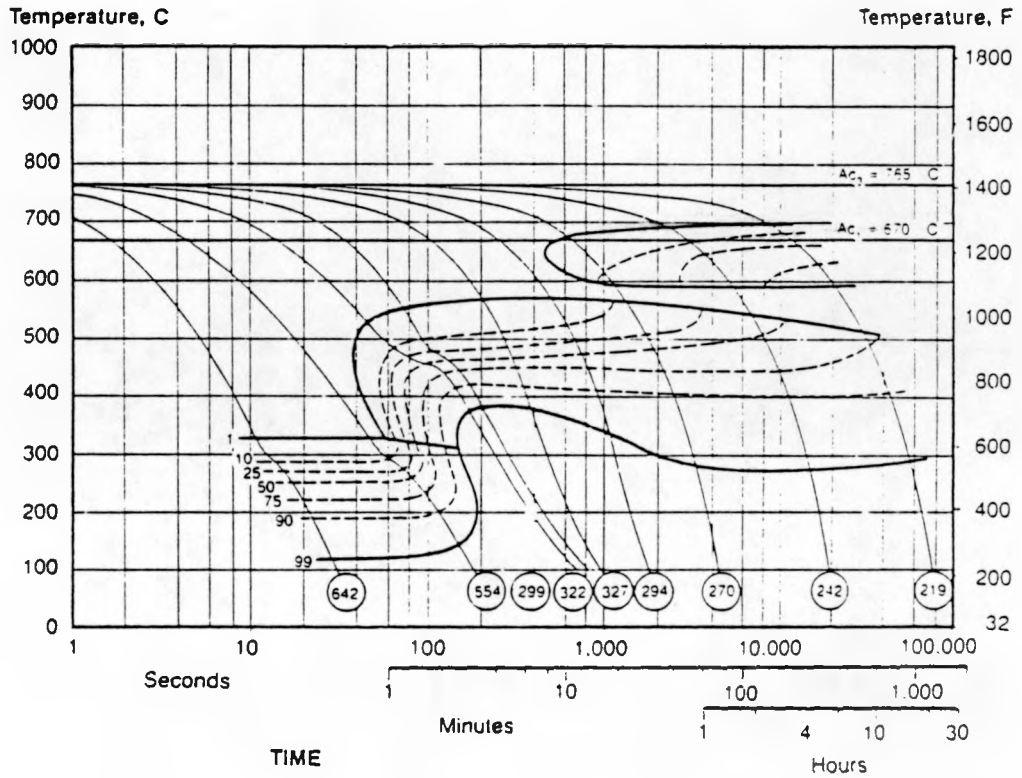

Figure 2. Continuous Cooling C-Curves for a Steel Containing 0.7%C, 0.36%Si, 0.84%Mn, 1.4%Ni and 0.47%Mo.

depending on the concentration of austenite-stabilizing alloying elements in the steels. Once the M_s is reached, further transformation takes place during cooling until the reaction ceases at the finish, M_f, temperature [11-14].

The morphology of martensite is found to be dependent on the carbon concentration in steel. Low carbon martensite, up to 0.5 wt% carbon, is referred to as lath or plate-like martensite. Above 0.5 wt% C, it is usually called acicular martensite. Addition of metallic alloying elements cause martensite to occur at much lower carbon contents, even for the carbon-free case [11,12]. As-transformed martensite is hard and brittle. It possesses relatively high strength but low ductility, so that, annealed and tempered martensite is required for practical applications.

Ferrite Structure

By studying the time-temperature-transformation (TTT) diagram and continuous-cooling transformation (CCT) diagram, we can find that high temperature austenite can transform into ferrite, pearlite, bainite, martensite or a mixture depending on the cooling rate. The higher the cooling rate the more favorable is the formation of bainite and martensite. The lower the cooling rate the more likely it is that ferrite and pearlite will be formed. When an intermediate cooling rate results, a mixture of ferrite and bainite or martensite is obtained.

When a 2 1/4 Cr-1Mo steel, typically bainitic structure, is cooled with a moderate rate from the austenite phase, a mixture of bainite and proeutectoid polygonal ferrite is formed as shown in Figure 3 [16].

Figure 3. Microstructure of a Standard 2 1/4Cr-1Mo Steel in Normalized and Tempered Condition.

R. L. Klueh and J. M. Vitek investigated the Modified 2 1/4 Cr steels and found that both 2 1/4 Cr steels with 0.25% vanadium addition and (1W+0.25V) addition had 30 to 35% proeutectoid polygonal ferrite and the rest was bainite. A fully bainitic structure was observed in 2 1/4 Cr-2W steel while with 0.25% V addition, 8 to 10% polygonal ferrite was observed in 2 1/4 Cr-2W-0.25V steel [17].

When a 12 Cr-1Mo steel, typically martensitic structure, was cooled from austenite, a mixture of martensite and ferrite could form depending upon the alloying elements present. Figure 4 shows the duplex phase structure of a 12Cr-1Mo-1W-V-Nb steel [9,18,19]. This ferrite is normally referred to as delta (δ) ferrite, which can have a continuous existence from the melting point to room temperature in this steel.

Figure 5 shows the binary iron-chromium equilibrium diagram [20]. As shown in this diagram, Cr restricts the occurrence of the gamma (τ) loop to the extent that above 13% Cr the binary alloys are ferritic over the entire temperature range. There is a narrow ($\alpha+\tau$) range between about 12% and 13% Cr. Yoshikawa et al. have reported that in a 0.1C-12Cr-1Mo-1W-1V-Nb (HCM12) steel, composed of 20-30% δ-ferrite and the balance tempered martensite, δ-ferrite tends to decrease the impact values. The higher content of Mo equivalent (Mo+0.5W) tends to increase δ-ferrite content and thus

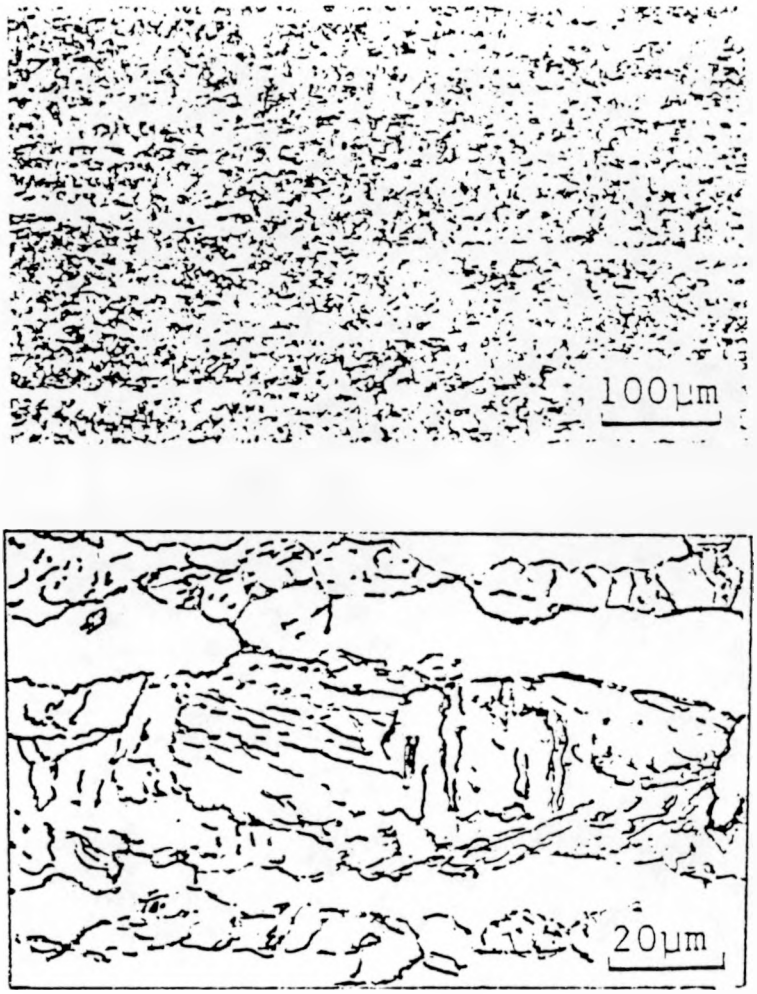

Figure 4. Microstructure of a 12Cr-1Mo-1W-V-Nb Steel in Normalized and Tempered Condition.

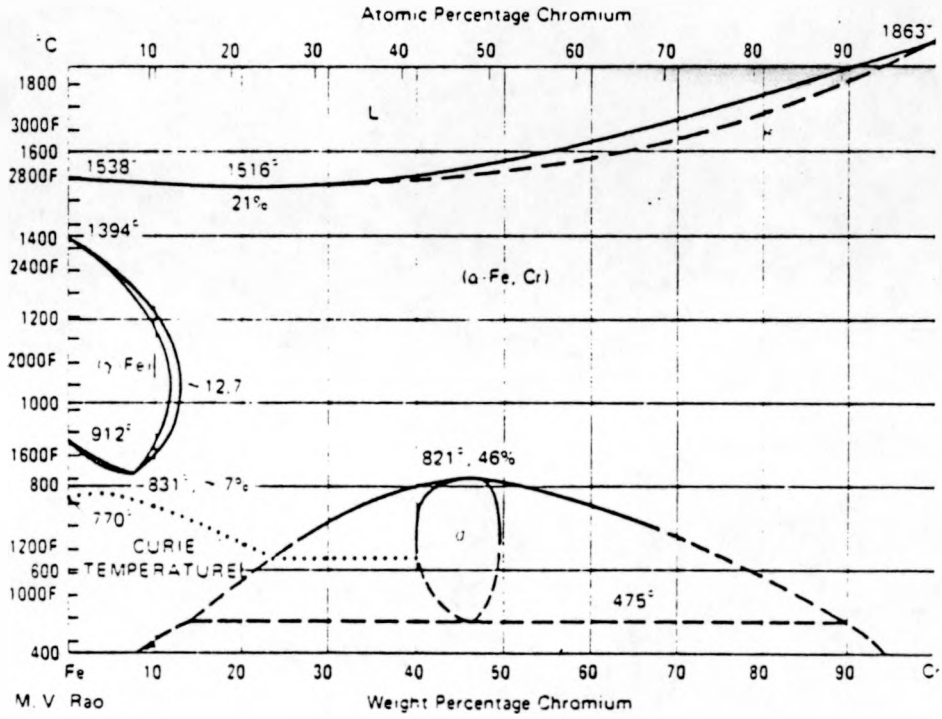

Figure 5. Equilibrium Iron-Chromium Binary Phase Diagram.

decreases the toughness and raises the ductile-brittle-transition-temperature (DBTT) [18]. Mo and W are effective strengthening elements in steels due to solution hardening. The effect is significant up to 1.5% Mo equivalent. Therefore, a compromise was required to obtain the optimum strength and toughness. Figure 6 shows the relation between δ-ferrite content and Charpy impact values for 12% Cr steels while the relation between Cr equivalent and δ-ferrite content for 12% Cr steel is given in Figure 7.

R. L. Klueh reported that 12Cr-2WV steel contains 26% δ-ferrite when annealed at 1050°C while 5% and 9% Cr-2WV steels show a fully martensitic structure. With addition of 2.8% and 5.6% Mn, the 12% Cr steel contains about 10% and less than 1% δ-ferrite respectively. Also, the addition of 0.2% C in this steel (base composition contains about 0.5% Mn and 0.1% C) will decrease the δ-ferrite content to about 5% in the microstructure. Although Mn additions significantly reduce the formation of δ-ferrite, the Mn concentration should be minimized if lithium is used as the coolant for the first wall in a fusion reactor. This is because of the high solubility of Mn in lithium [21].

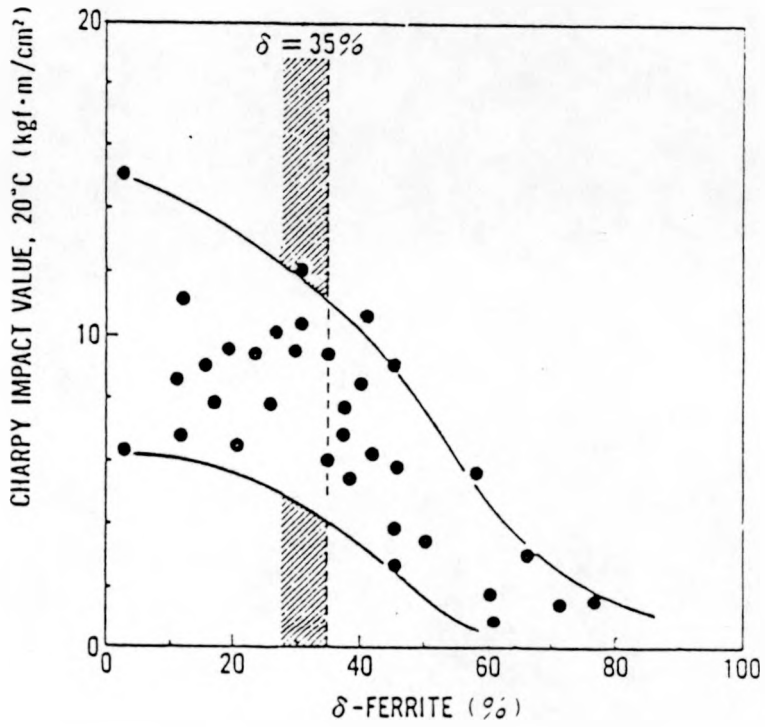

Figure 6. Relation Between δ-Ferrite Content and Charpy Impact Values for 12Cr Steel.

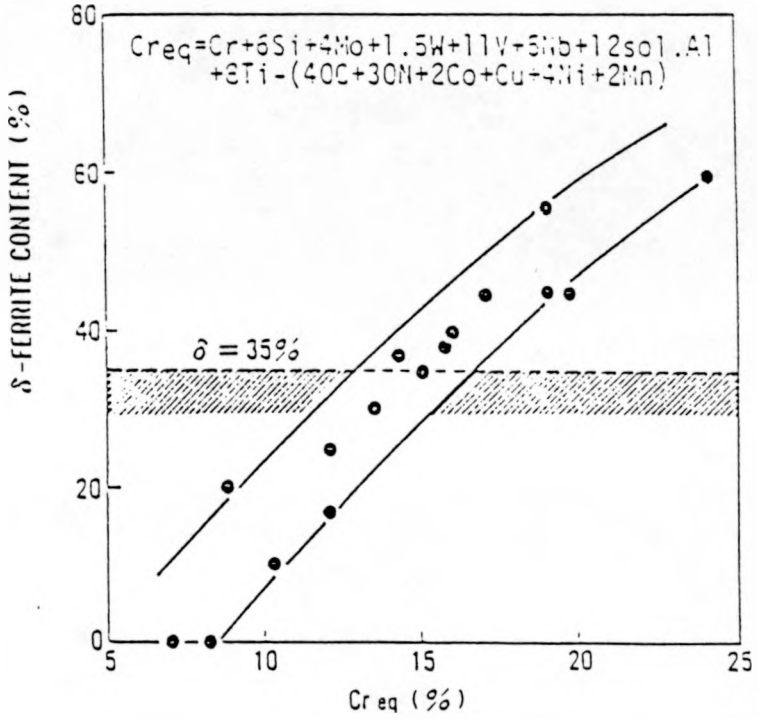

Figure 7. Relation Between Cr-Equivalent and δ-Ferrite Content For 12 Cr Steel.

Grain Size Effect

A well-known relationship between yield stress and grain size is expressed by the Hall-Petch equation of the form

$$\sigma_y = \sigma_0 + kD^{-\frac{1}{2}} \quad \text{------(5)}$$

where σ_y is the yield stress, σ_0 a frictional stress required to move dislocations, D is the grain size and k is a constant.

By reducing the grain size, we increase the number of grains and hence increase the amount of grain boundaries. Any dislocation moves only a short distance before encountering a grain boundary and the strength of the material is increased. Figure 8 shows the effects of grain size on the yield strength of a steel at room temperature [22]. Where σ_0 is the intercept on the stress axis. This stress is particularly sensitive to temperature and composition. The constant k represents the slope of the plot, which is sensitive to temperature, composition and strain rate.

Decarburization

When steel is heat-treated in an oxidizing atmosphere such as ambient air, the carbon tends to react with CO_2 and

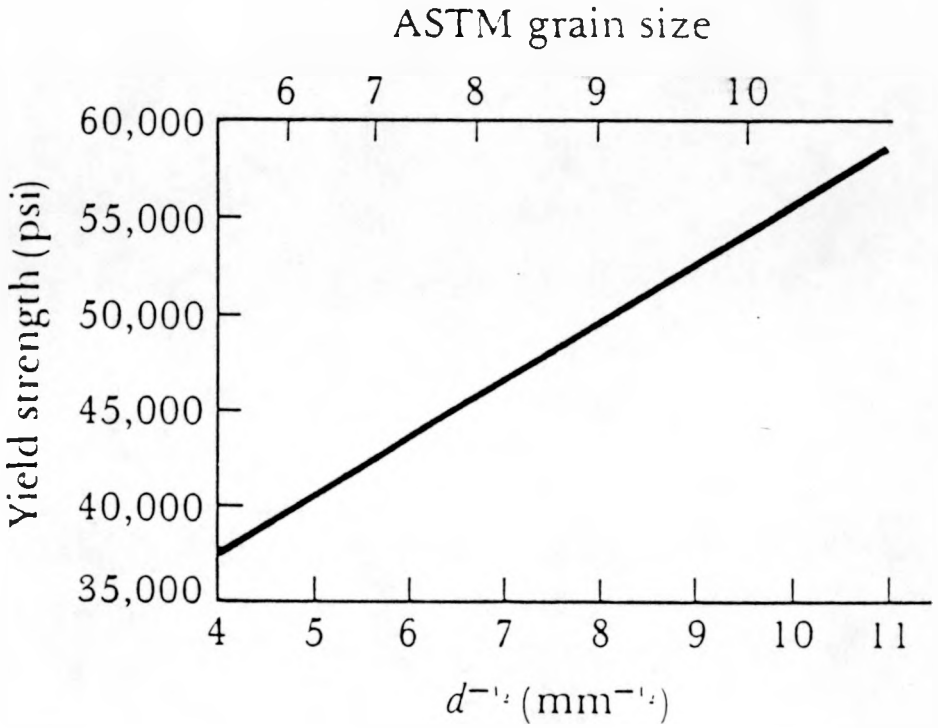

Figure 8. Effect of Grain Size on the Yield Strength of a Steel at Room Temperature.

be depleted from the surface of the steel. The reaction is as follows:

$$C + CO_{2(g)} \text{ ---> } 2CO_{(g)} \quad \text{------(6)}$$

where C is the depleted carbon in the steel surface layer. This low carbon surface layer reduces the mechanical properties of the steel at the surface. Decarburization is a diffusion-controlled thermally activated process. The diffusion coefficient of carbon atoms within steel plays an important role in this process.

The variation of carbon concentration in the decarburization process is expressed by the equation

$$C(x,t) = C_0 * \text{erf}\left(\frac{x}{2\sqrt{Dt}}\right) \quad \text{------(7)}$$

where C(x,t) is the carbon concentration at location x below the surface after time t, and C_0 is the initial uniform carbon concentration. The term "erf" is short for "error function", and D is the diffusion coefficient of carbon atoms. The above equation is satisfied, provided the diffusion coefficient is not a function of carbon concentration and the carbon concentration at the surface is effectively zero [23].

A different approach for estimating the depth of decarburization layer in tempering is used since most of the carbon is in the form of carbides and is strongly bonded.

It is practical to assume the diffusion of carbon in carbides is zero. The depth of decarburization layer in tempering treatment is expressed as follows by solving the moving boundary problem [24,25]

$$x = (2DtC_1/C_2)^{1/2} \quad \text{------(8)}$$

where x is the depth of total decarburization layer, D is the carbon diffusion coefficient in ferrite, t is the time for tempering, C_1 is the carbon solubility in ferrite and C_2 is the total carbon content of the material. The carbon solubility in ferrite from 400-727°C is expressed by

$$C_1 = 198 * \exp\left(\frac{-9117.5}{T}\right) \quad \text{------(9)}$$

where T is the absolute temperature in degrees kelvin of interest and C_1 is in weight percent.

The diffusion coefficient is given by

$$D = D_0 * \exp\left(\frac{-Q}{RT}\right) \quad \text{------(10)}$$

where Q is the activation energy (cal/mol), R is the gas constant (1.987 cal/mol/°K), T is the absolute temperature and D_0 is a constant for a given diffusion system. Some typical values for activation energies and constant D_0 are shown in Table 3 [22].

The error function is defined by the integral

$$\mathrm{erf}(x) = \frac{2}{\sqrt{\pi}} * \int_0^x \exp(-y^2)\,dy \quad \text{------(11)}$$

It can also be expressed by the following equation [26]:

$$\mathrm{erf}(x) = \frac{2}{\sqrt{\pi}} * \left(x - \frac{x^3}{1!3} + \frac{x^5}{2!5} - \frac{x^7}{3!7} + \frac{x^9}{4!9} - \cdots\right)$$

$$= \frac{2}{\sqrt{\pi}} * \left(x + \sum_{n=1}^{n=\infty} \frac{(-1)^n * x^{2n+1}}{n! * (2n+1)}\right) \quad \text{------(12)}$$

Properties of Cr Steels

A series of low activation ferritic steels, including 2 1/4, 9 and 12% Cr steels, have been studied by H. T. Lin and B. A. Chin [9]. The results show that sound autogenous GTAW welds can be obtained on all the low activation ferritic steels with no cracks or any defects observed. 2 1/4 Cr steels primarily consist of a mixture of bainite and proeutectoid polygonal ferrite while 9% and 12% Cr steels are in principle martensitic structures. Both carbon and vanadium exhibit the tendency to promote the proeutectoid polygonal ferrite or δ-ferrite in all steels. Ghoniem

Table 3. Diffusion Data for Selected Metals [22].

Diffusion Couple	Q (cal/mol)	D_0 (cm^2/s)
Interstitial Diffusion		
C in FCC Iron	32,900	0.23
C in BCC Iron	20,900	0.011
N in FCC Iron	34,600	0.0034
N in BCC Iron	18,300	0.0047
H in FCC Iron	10,300	0.0063
H in BCC Iron	3,600	0.0012
Self-Diffusion		
Au in Au	43,800	0.13
Al in Al	32,200	0.10
Cu in Cu	49,300	0.36
Fe in FCC Iron	66,700	0.65
Fe in BCC Iron	58,900	4.1
Heterogeneous Diffusion		
Ni in Cu	57,900	2.3
Cu in Ni	61,500	0.65
Zn in Cu	43,900	0.78
Al in Cu	39,500	0.045
Ni in FCC Iron	64,000	4.1

reported that carbon atom diffusion rates are much higher in 2 1/4% Cr steels which are composed of the bainitic structure. Steels with higher Cr content have a lower carbon atom diffusion rate which yields a martensitic structure easily formed by the diffusionless shear process [27].

A larger variation in traverse microhardness was found for 9% and 12% Cr steels while a higher impact strength was observed for 2 1/4 Cr steels welds in Lin and Chin's report. In their investigation, weld bend test results for 2 1/4% and 9% Cr steels were all satisfactory, yet 12% Cr steels failed at the fusion zone. This suggests that post-weld heat treatment is needed in the 12% Cr steels to restore the ductility and toughness. HAZ and base metal interface failures were found for 2 1/4% Cr steels in tensile tests, whereas 9% and 12% Cr steels failed in the base metal.

A newly developed 12Cr-1.5Mo-1W steel has been studied by Vineberg et al. This steel consists of 15 to 25% δ-ferrite with the balance martensite in the normalized and tempered condition. This duplex structure steel effectively eliminates weld cracking susceptibility in fusion welding without the need for preheat or post-weld stress relief treatment. 12Cr-1Mo-V steels typically show extensive cracking when not preheated [28]. Tensile properties of the welds for this steel match the base metal and adequate impact toughness of the weld is observed. A similar result

was obtained by Hilderbrand et al. in commercial 12C-1Mo-0.3V-0.5W Sandvik HT-9 steel [29].

D. S. Gelles et al. have studied the fracture toughness of HT-9 and 9Cr-1Mo welds with compact tensile specimens [30,31]. The results show overall fracture toughness of the welds for both steels is not significantly reduced by welding. The toughness was found to decrease with increasing test temperature. However, a decrease in the tearing modulus of all welds compared to those of base metals was observed indicating that both alloys have less crack propagation resistance as a result of welding.

A 9Cr-1Mo steel modified with niobium and vanadium was investigated by Sikka [32]. This modified steel shows a fully martensitic structure, free of ferrite, under normalized and tempered conditions (1040°C for 1 hour, air cooled to room temperature; 760°C for 1 hour, cooled to room temperature). This steel has been shown to be not susceptible to hot cracking. Hydrogen sensitivity was also prevented by preheating to a temperature of 200°C. Both Nb and V improve the elevated-temperature strength of this steel. King and David also showed that the welds of the modified steel had a better tensile strength than the base metal after electron beam welding [33].

The mechanical properties for Cr-W steels studied in this work have been extensively investigated [17,21,34-38]. These Cr-W steels are patterned after the conventional

ferritic, 2 1/4 Cr-1Mo, 9 Cr-1MoVNb and 12 Cr-1MoVW, being considered as candidates for fusion reactor structural components. Heat treatment studies indicate that the newly developed steels have tempering characteristics similar to the conventional ferritic steels. Comparable tensile properties in 2 1/4 and 9 Cr-Mo steels were obtained for the Cr-W steels when both received similar normalization and tempering treatments. This result supports the initial concept of alloying elements replacement. Tensile properties were degraded in 12Cr-2WV steel due to δ-ferrite formation in its structure. A summary of the impact properties of Cr-W steels is given in Table 4. The results indicate that Cr-W steels have better impact properties than conventional Cr-Mo steels. Inferior impact properties were found in 2 1/4Cr-2WV than high Cr Steels. This was attributed to microstructure. By proper alloying to increase hardenability and heat treatment, it was argued that the impact properties of 2 1/4Cr-2WV can be improved.

Table 4. Summary of Impact Properties For Cr-W Steels [38].

Steel	Tempering Temperature[b] (°C)	Impact Properties[a] TT_{41J} (°C)	TT_{68J} (°C)	TT_{LE} (°C)	USE (°C)
2.25CrV	700	85	86	85	240
	750	66	69	70	318
2.25Cr-1WV	725	52	53	52	220
	750	8	23	38	340
2.25Cr-2W	700	24	24	12	260
	750	-41	-30	-31	324
2.25Cr-2WV	700	85	110	112	131
	750	31	31	31	265
5Cr-2WV	700	-61	-46	-46	219
	750	-97	-76	-83	259
9Cr-2WV	700	7	26	33	157
	750	-69	-49	-42	217
9Cr-2WVTa	700	-47	-24	-20	181
	750	-95	-78	-82	258
12Cr-2WV	700	11	20	19	168
	750	-13	-2	-24	193
9Cr-1MoVNb	700	56	68	68	161
	750	27	41	41	199
12Cr-1MoVW	700	33	68	64	99
	750	4	29	26	115

[a] TT_{41J} is 41-J (30 ft-lb) transition temperature; TT_{68J} is 68-J (50 ft-lb) transition temperature; TT_{LE} is lateral expansion transition temperature as determined by 0.889 mm expansion; USE is upper shelf energy.

[b] All steels were tempered for 1 h; before tempering all steels but the 2.25Cr-2W were normalized at 1050°C; the 2.25Cr-2W was normalized at 900°C.

III. EXPERIMENTAL PROCEDURE

Materials Fabrication

Eight heats of low activation ferritic steels patterned after commercially available chromium-molybdenum alloys were investigated in this study. These steels, prepared by Combustion Engineering, Inc., were received from Oak Ridge National Laboratory, Tennessee.

All the steels were produced by air-melting and then electroslag remelting (ESR) to obtain ingots about 18 kg in size. The ESR ingots were hot rolled to different thicknesses according to specific use. Materials were used in the normalized and tempered condition. All but heat 3787 were normalized 0.5 hour at 1050°C and air cooled. Heat 3787 was normalized 0.5 hour at 900°C and then air cooled. Higher austenization treatments were used for all steels, except heat 3787, to ensure that the vanadium carbides present were dissolved. Tempering was performed for 1 hour at 700°C for all steels.

Dimensions of the as-received materials are shown in Table 5. In order to obtain the proper thickness for use in tensile specimens produced by a punch and die, as-received materials were hot-rolled. These steels were heated at 700°C in an argon atmosphere, using a Blue M model TS-15-1

furnace, followed by hot rolling to the final thickness of 0.76 mm. Rolling was done in the as-received rolling direction, using a Stanat TA-215 rolling mill, manufactured by Stanat MFG. Co. Inc., Westbury, NY. Steels were then sectioned into 0.76 mm x 43 mm x width (as-rolled) plates.

Table 5. Dimensions of As-Received Materials (mm)

Heat No.	Thickness	Width	Length
3785	2.00	104	152
3786	1.75	106	149
3787	2.85	98	164
3788	2.60	106	151
3789	2.60	101	150
3790	3.30	99	151
3791	3.20	106	150
3792	3.10	104	152

Heat Treatment

As-rolled materials were heat-treated to restore the mechanical properties. The furnace used to perform the heat-treatment was a Blue M Electric Company Model 8625C-3 Stabil-Glow Box Type Furnace, with a solid state proportional control system. The furnace was preheated for 6 hours in an argon atmosphere to ensure thermal equilibrium was reached. All heats except heat 3787 were annealed at 1050°C for 0.5 hour then water quenched. Heat 3787 was annealed at 900°C then quenched. Tempering was performed for 1 hour at 700°C for all heats after quenching.

In order to reduce oxidation, all plates were wrapped with zirconium foil and put into an alumina crucible, 68 mm diameter and 144 mm in height. The crucible was purged with argon gas from the bottom for 2 hours then covered with a lid. The gas flow was controlled by a glycerin bubbler. Gas bubbles were maintained discrete to reduce stirring with air. The loaded crucible was then moved into the furnace and placed on the tip of a K-type thermocouple (chromel and alumel). The thermocouple was used to ensure plates inside the crucible had experienced the exact temperature needed for heat treatment. The above procedures were conducted in both annealing and tempering treatments.

Bead Blasting

The as-heat-treated plates formed an oxidation film on both surfaces despite the use of as an argon atmosphere. A Dry Blast System, manufactured by Skat Blast,Inc., Canfield, OH, was used to remove the oxidation layers. The abrasive used for blasting was sodium aluminum silicate base glass beads manufactured by Flex-O-Lite Inc., St. Louis, MO. The size of glass beads was in the range of 60 to 80 mesh.

Welding Process

Autogenous bead-on-plate welds were produced using the gas tungsten arc welding (GTAW) process to evaluate the weldability for all steels. The welding power supply was a Miller Synchrowave 500 AC/DC welding power source which is manufactured by Miller Electric MFG. Co., Appleton, WI. Table 6 shows the settings of the welding power supply in this study. The water-cooled torch was manipulated using a Heath Engineering Company ESAB X-Y positioning table, model No. MCD/600-MODFD, controlled by a ECT-150 Tracing Control System, manufactured by Steward-Warner Electronics, Chicago, IL. The electrodes used were 1/16" diameter 2% thoriated tungsten electrodes.

Plates were first cleaned with acetone to prevent surface contamination before welding was performed and all edges were flushed. Welds were produced in a protective argon atmosphere (both top and bottom) under a fully constrained condition. The argon protective gas was held in

place by a plexiglass chamber which helped to reduce oxidation during the welding process. Weld plates were laterally constrained using two pieces of 11 mm square plain carbon steel bar during welding. This was used to simulate the restraint condition encountered in the maintenance and repair of structural components. In order to initiate and terminate the arc, two pieces of plate (start and runoff tabs) were placed in front and in back of the weld plates so a uniform weld could be obtained for the entire length of plates. The welding station is shown in Figure 9.

Table 6. Welding Power Supply Settings

1. Contractor	Remote
2. Current	Remote
3. Hi Frequency	On
4. Crater Fill	Out
5. Start Current	On, 1 A
6. AC Balance	Balanced
7. Post Flow Time	6 Second
8. Polarity	DC, Straight
9. Pulser	Out

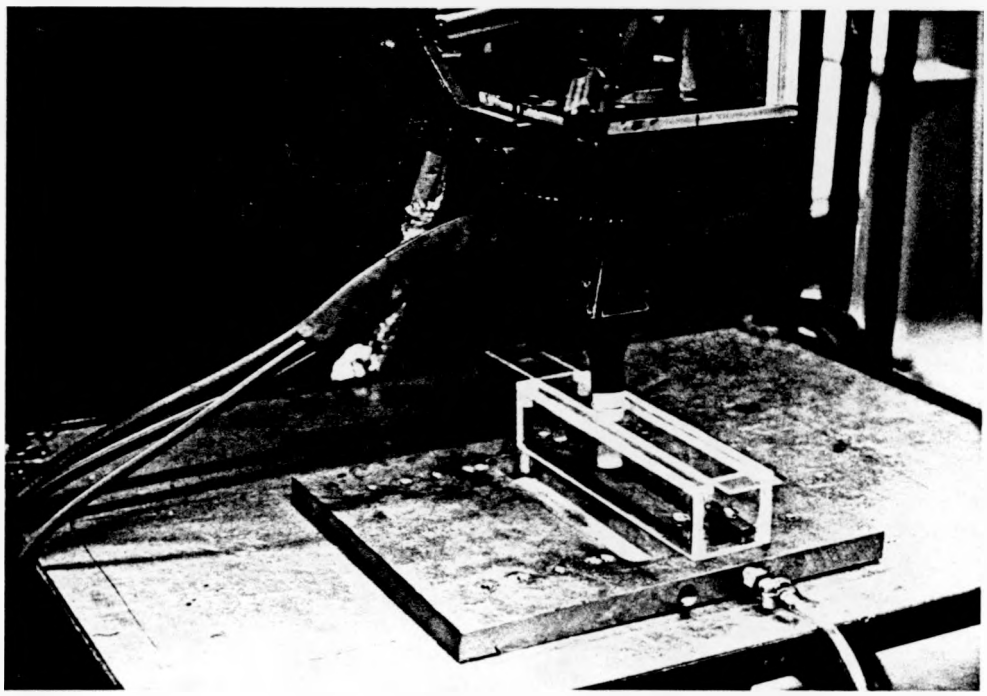

Figure 9. Welding Station Setup.

Welding process parameters used to obtain full penetration in the study were 10 V-DC, 38 A. Torch travel speed was 4.6 mm/sec with an argon gas flow of 20 cu.ft/hr from the torch and 10 cu.ft/hr from the bottom. Table 7 summarizes the welding conditions used in this study. The welding heat input, defined by voltage multiplied by current divided by torch travel speed, is 82.6 J/mm. A full penetration weld with approximately a 2.5 mm fusion zone was obtained perpendicular to the rolling direction.

Table 7. Conditions for Full Penetration Welding

1. Current	38 A
2. Voltage	10 V
3. Polarity	DC, Straight
4. Torch Speed	4.6 mm/sec
5. Shielding Gas	Ar
6. Gas Flow:	
a. Top	20 Cfh
b. Bottom	10 Cfh, Continued
7. W-Electrode	1/16" Diameter
	2% Thoriated
8. Fully Constrained	

Microstructure Characterization

The weld plates were sectioned into 0.76 mm x 8 mm x 43 mm specimens transverse to the welding direction. This dimension includes all structural features of the weld (fusion zone, heat affected zone and base metal) for microstructure and transverse microhardness characterizations. Specimens were first hot-mounted in phenolic powder followed by mechanical grinding, using silicon carbide grinding papers down to 4000 grit. For final polishing, 0.05 micron alpha alumina mixed with distilled water was used. The etching solution used in this investigation contained one part of HNO_3, two parts of HF and three parts of glycerin.

The microstructure was observed using a MC-63 Ziess Optical Microscope over the entire specimen including FZ, HAZ and BM. A Microcomp Image Analysis System, model No. NC-655, associated with the microscope was used to measure the ferrite volume fractions present.

DPH Microhardness Characterization

As a means to ascertain microstructure-properties relationships, traverse diamond pyramid microhardness (DPH) measurements were conducted across the weld regions, using a LECO DM-400 Hardness Tester. A diamond pyramid indenter was used with a load of 50 grams for a duration of 12 seconds. The indentations had a diagonal length from 10 to 20 μm

depending on the phases present and chemical composition of the specimens. Measurements were obtained in a 4 x 30 array arrangement as shown in Figure 10. Measurements were 0.1 mm away from one another so that the effect of strain hardening caused by neighboring indentations was negligible. The measurements close to surfaces also were a minimum of 0.1 mm away from the surface to avoid edge effects.

Electropolishing

Specimens prepared for subsequent bending and tensile tests had the weld reinforcements mechanically ground off flush with the surface of the base metal and then the specimens were electropolished prior to testing. Electropolishing was conducted using a Buehler No.70-1730 Electromet III Polisher/Etcher. The electrolyte contained 30 ml of 70% perchloric acid and 270 ml methanol. The electropolishing was conducted under 1.4 V, 0.5 A for 45 sec with a stainless steel electrode. Temperature of the process was 0°C, controlled by using liquid nitrogen.

Weld Bend Test

The three-point guide-bend test was used as an index to evaluate the weld soundness. Specimens used in this test had a dimension of 0.76 mm x 8 mm x 43 mm. As-electropolished specimens were etched prior to test using the same solution used for metallographic observation. This etchant aided in identifying where the fracture occurred.

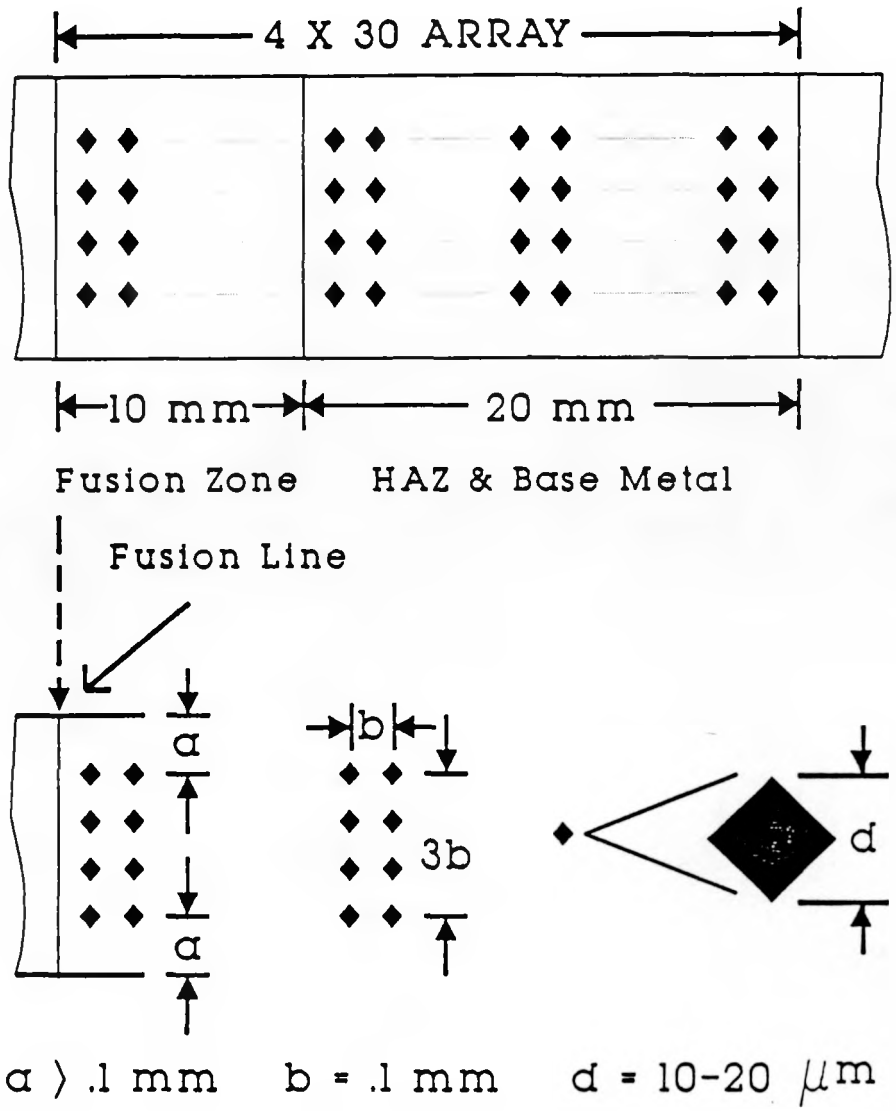

Figure 10. Arrangement of Microhardness Measurement.

In order to evaluate the soundness of the weld, face-bend tests were conducted in this study. The initial three-point bend was made on a model 1125 Instron Machine, equipped with a screw-driven crosshead. A plunger head traveled toward the fusion zone to produce an angle of approximately 100°. The crosshead had a travel speed of 0.508 mm/min and the supporting span distance was 20 mm. The final bend was performed with a vise. Initially bent specimens were placed in between two heads of the vise. Distance between the two heads was then decreased slowly without abrupt shock. A 1.5 mm thick space bar was placed in between two ends of the specimen. During the test, special care was taken so that the load on both ends of the specimen would maintain a symmetric loading distribution in the fusion zone. This ensured that appropriate results were obtained. Testing was performed until the specimen broke into two pieces or laterally contacted with the space bar (i.e. 180° bend). Figure 11 shows the setups for initial and final bending tests.

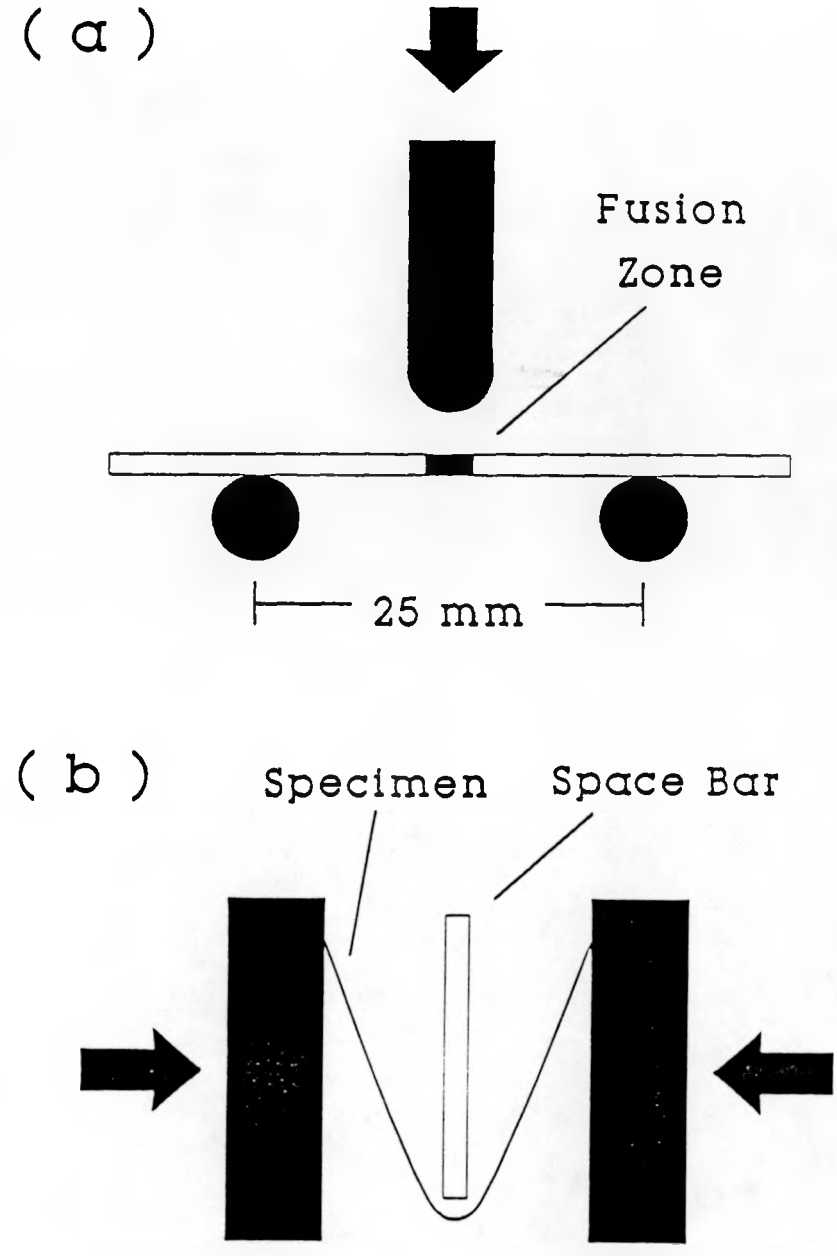

Figure 11. Configurations of Weld-Bend Test: (a) Initial Bend, (b) Final Bend.

Tensile Test

Tensile test specimens were made with a punch and die at ORNL. Specimens were cut perpendicular to the weld and had a reduced gage section of 12.7 mm long by 3.175 mm wide by 0.76 mm thick. Figure 12 shows the dimensions of the tensile specimens tested in this study. All the specimens were prepared using the same grinding, polishing and etching procedures that the bending test specimens received.

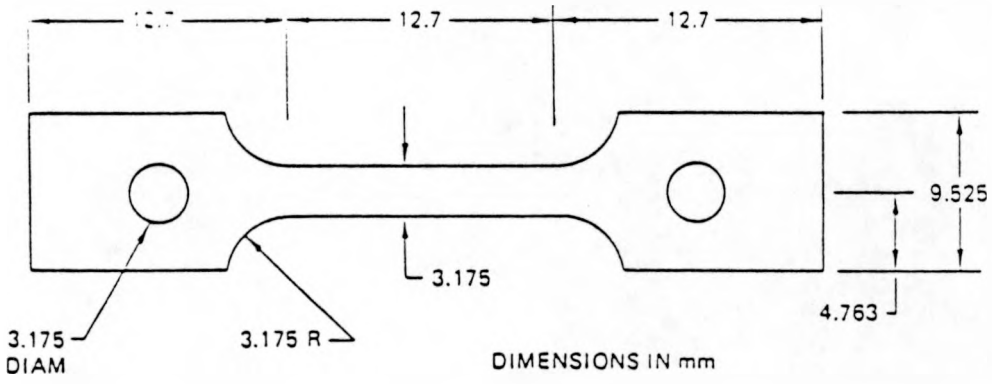

Figure 12. Schematic of Tensile Test Specimens.

Generally, strain rate plays an important role in the tensile properties and fracture mechanisms of a material. Strain rate is defined as the ratio of crosshead speed divided by gage length. Materials subjected to a higher strain rate tend to show an increase in yield strength and ultimate tensile strength. Ductility, on the other hand, typically decreases when strain rate is increased and brittle fracture mechanisms dominate. The static tension test has a typical strain rate from 10^{-5} to 10^{-1} sec^{-1} for a screw-driven machine [39]. In this study, tensile tests were performed on an Instron Machine with a crosshead speed of 0.508 mm/min which resulted in a strain rate of 6.67×10^{-4} sec^{-1}. All tests were conducted at room temperature.

SEM Fractography Observation

The fracture morphology examinations were carried out with a JOEL 840 Scanning Electron microscope (SEM) to investigate the fracture mechanisms and deformation of the weld bend tested specimens. All the observations were conducted at 15 KV accelerating voltage.

IV. EXPERIMENTAL RESULTS

Microstructure Characterization

Microstructures of as-welded specimens were examined by optical microscopy. The ferrite content was investigated using an image analysis system associated with the optical microscope. Diamond pyramid hardness (DPH) was measured across the weld region.

Gas tungsten arc welding was performed for all heats under quenched and tempered condition. All heats, except 2 1/4 Cr-2W steel, were austenitized at 1050°C for 0.5 hour then water quenched. 2 1/4 Cr-2W steel was austenitized at 900°C for 0.5 hour and then quenched. All heats were tempered at 700°C for one hour after quenching. The as-welded microstructure consists of four distinct regions which are as follows for all heats: fusion zone, heat-affected zone (grain-growth region and grain-refined region) and unchanged base metal. Experimental results reveal that all the steels are free of cracks and readily weldable.

Figures 13-16 show the microstructure at each region across the weld for 2 1/4 Cr low activation ferritic steels in the as-welded condition. Optical micrographs show that 2 1/4 Cr steels are basically bainitic steels with different

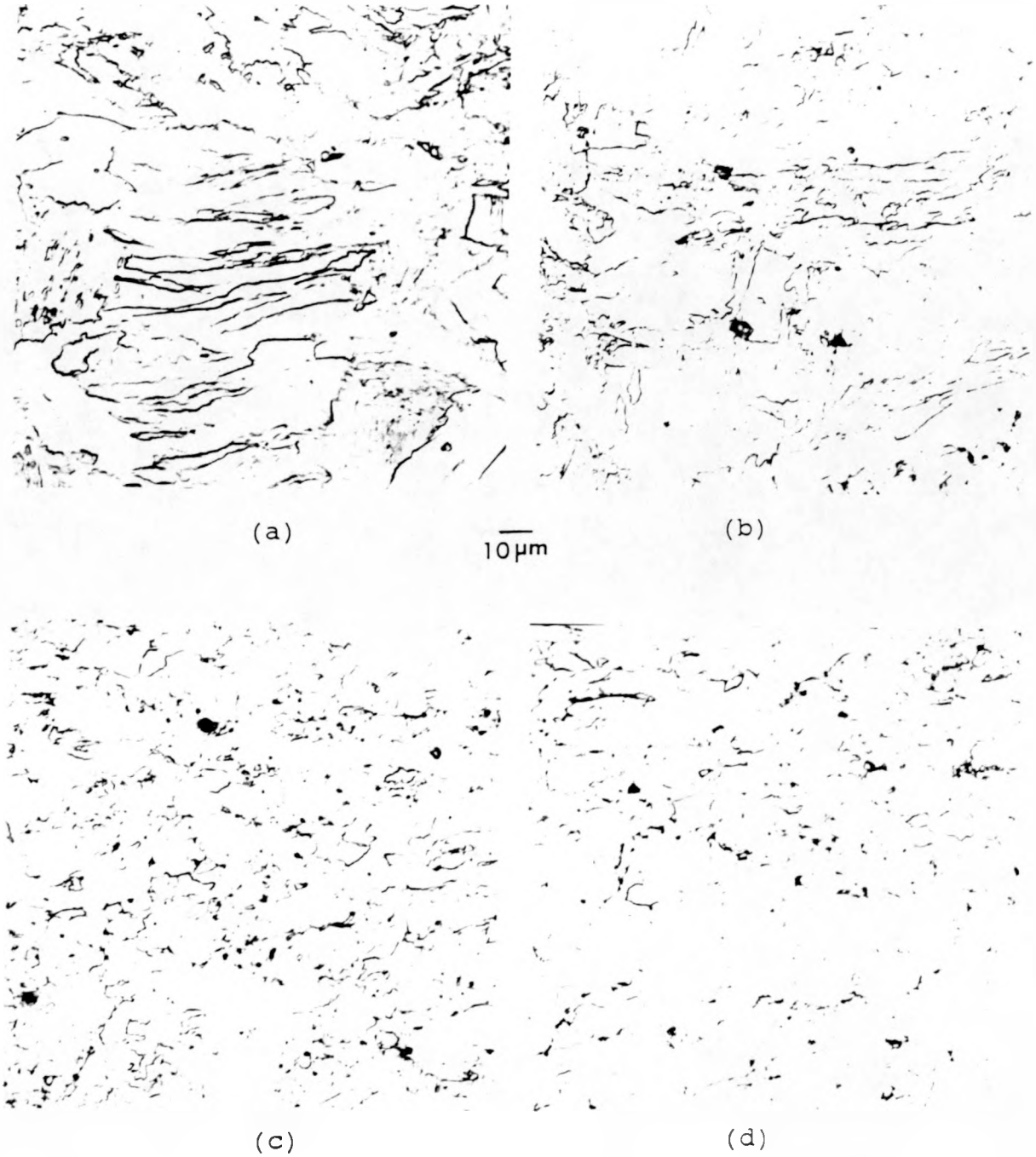

Figure 13. Optical Microstructure of 2 1/4 CrV Steel: (a) Fusion Zone (b) Grain-Growth Region (c) Grain-Refined Region (d) Base Metal.

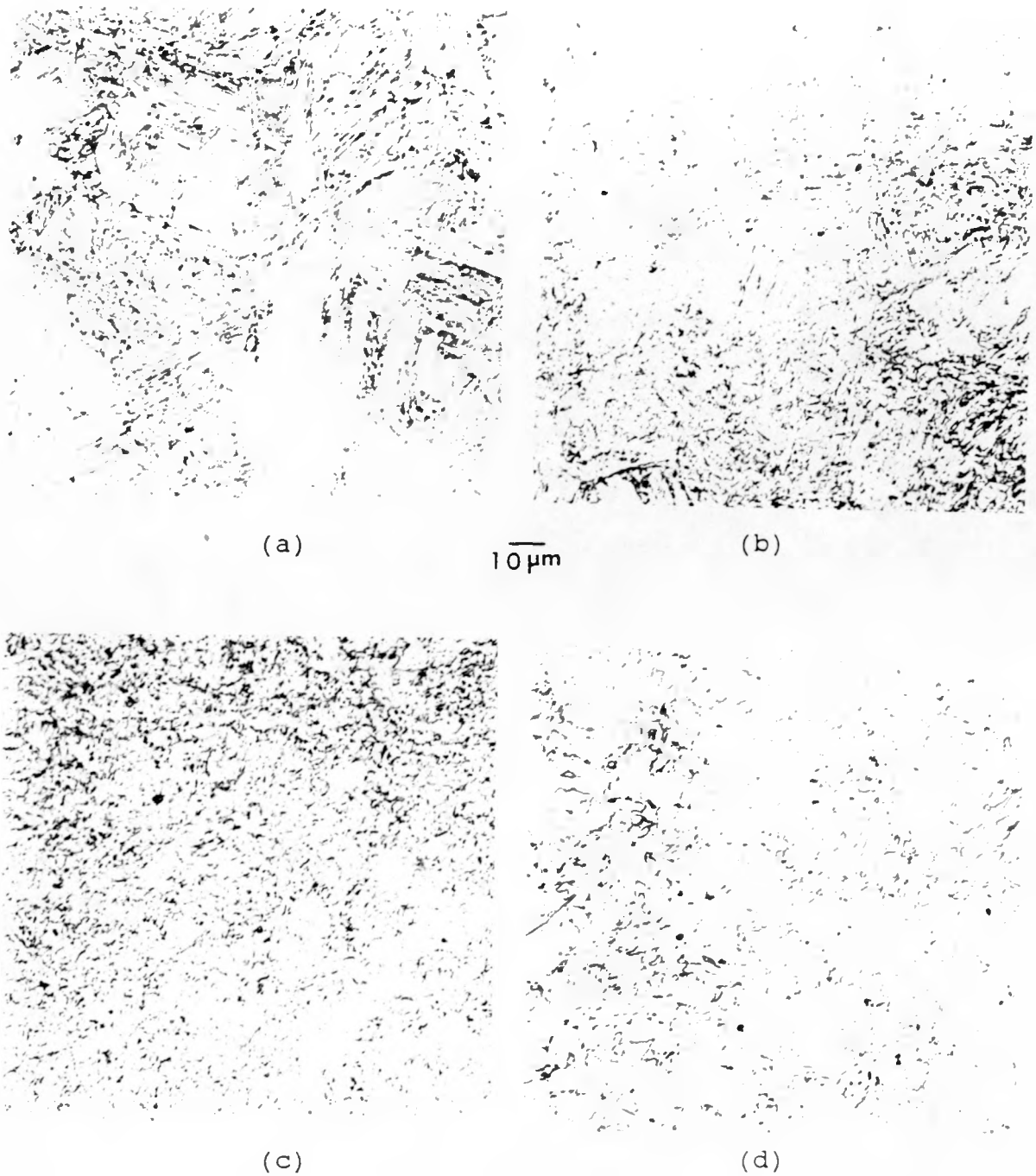

Figure 14. Optical Microstructure of 2 1/4 Cr-1WV Steel: (a) Fusion Zone (b) Grain-Growth Region (c) Grain-Refined Region (d) Base Metal.

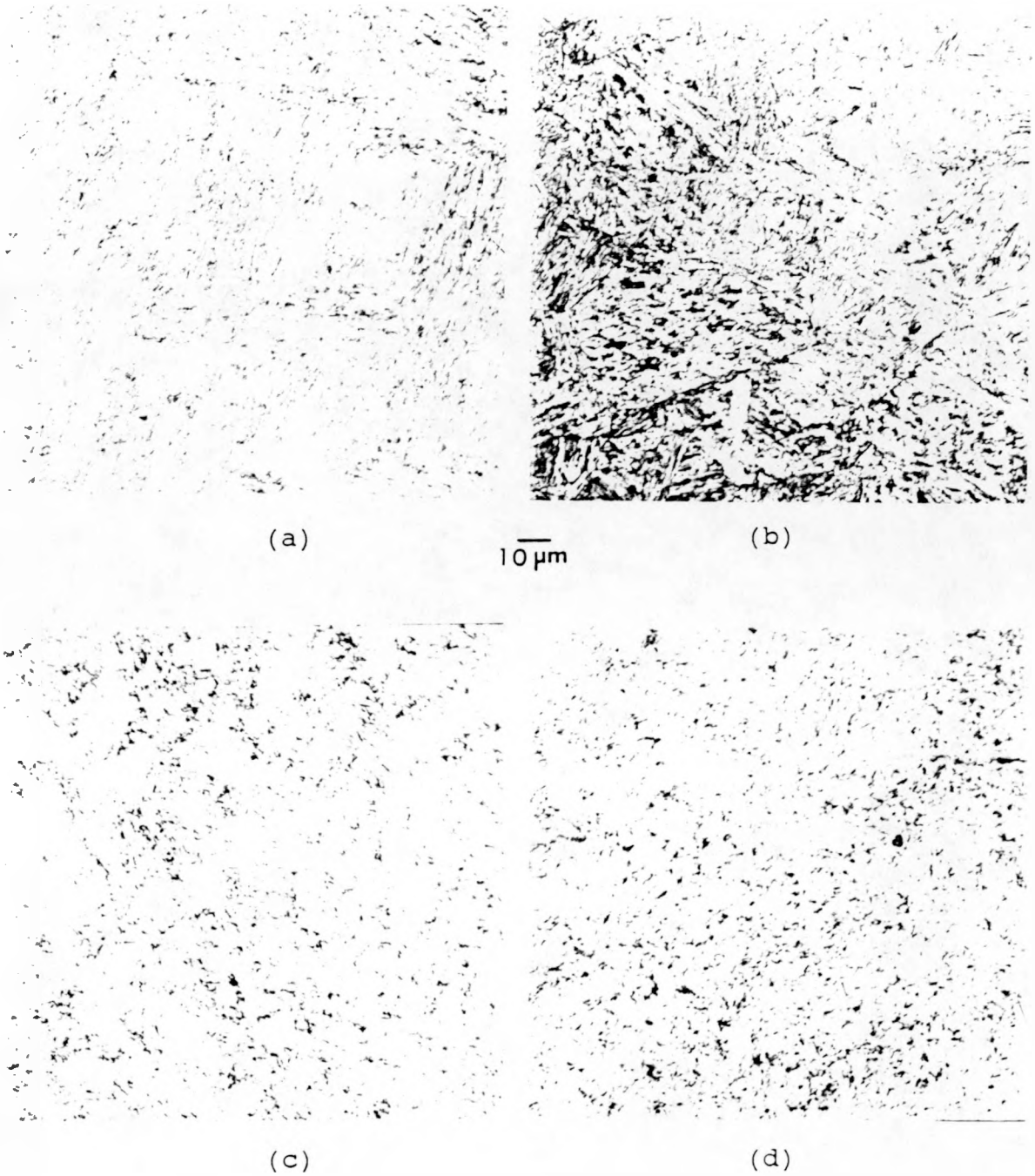

Figure 15. Optical Microstructure of 2 1/4 Cr-2W Steel: (a) Fusion Zone (b) Grain-Growth Region (c) Grain-Refined Region (d) Base Metal.

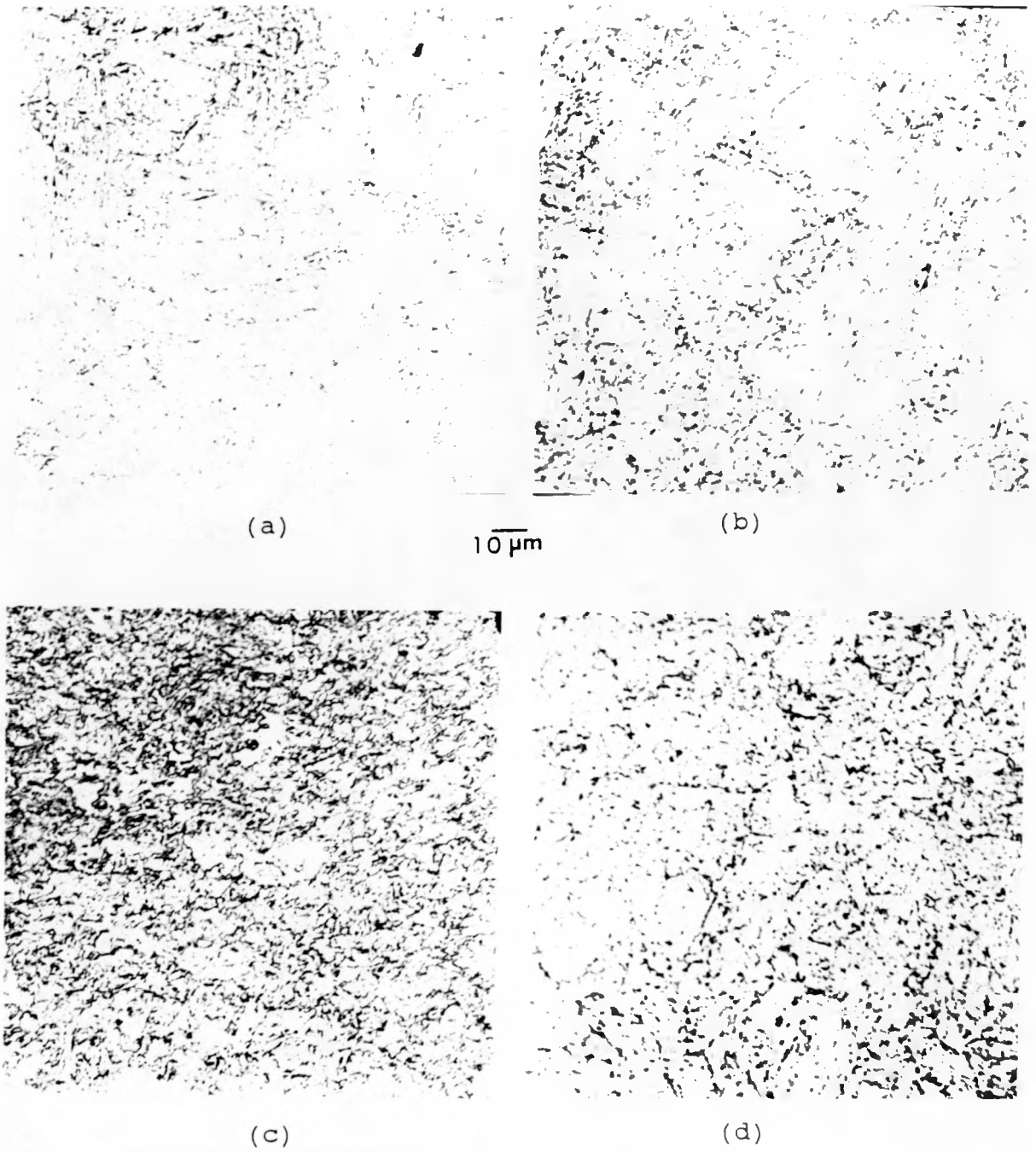

Figure 16. Optical Microstructure of 2 1/4 Cr-2WV Steel: (a) Fusion Zone (b) Grain-Growth Region (c) Grain-Refined Region (d) Base Metal.

amounts of proeutectoid polygonal ferrite at the base metal depending on the chemical composition. 2 1/4 Cr-V steel contains 8-12% polygonal ferrite with the rest being bainite, while 2 1/4 Cr-1WV steel consists of 5-10% ferrite. As the tungsten content increased, 2 1/4-2WV steel had an even lower ferrite content of 3-8%. Without the vanadium addition, 2 1/4-2W steel is fully bainite and possessed a finer grain structure than the other 2 1/4% Cr steels.

The 5 and 9% Cr steels consist of a completely martensitic structure. A dual phase structure is observed in 12 Cr-2WV steel in the quenched and tempered condition is composed of 12-17% delta ferrite with the remainder being martensite. Figures 17-20 show the optical microstructure for 5-12% Cr steels in different regions in the as-welded condition. A list of microstructures for the low activation ferritic steels studied in this work, under quenched and tempered conditions, is shown in Table 8. These structures are those found in the base metal under the as-welded condition for each material in Figures 13-20.

Diamond pyramid microhardness (DPH) measurements for each heat across the weld with corresponding microstructures are presented in Figures 21-28. Each microhardness profile shown in Figures 21-28 is from 4 x 30 array of data. Each point represents an average of four measurements located the same distance away from fusion line. These data are the

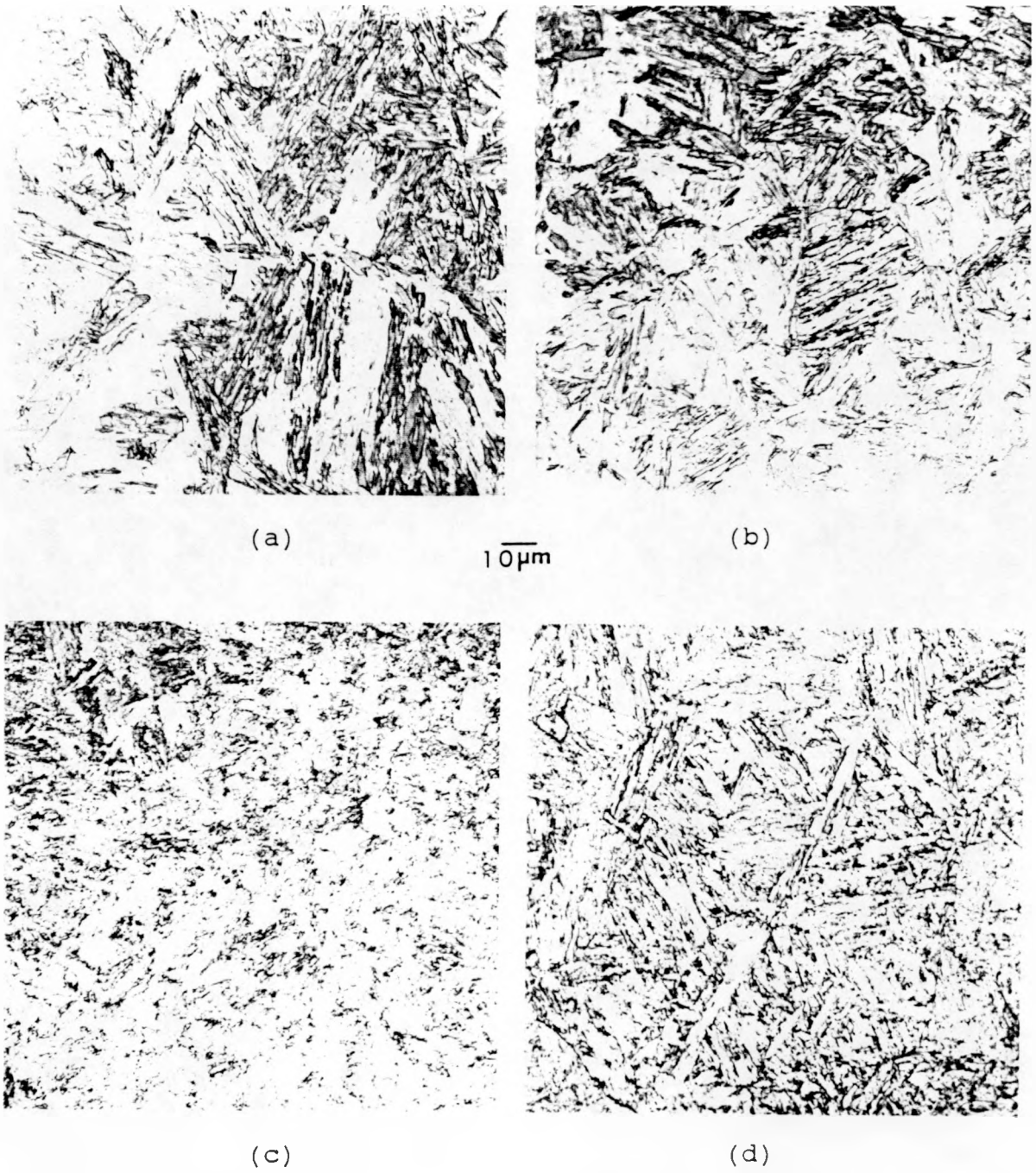

Figure 17. Optical Microstructure of 5 Cr-2WV Steel: (a) Fusion Zone (b) Grain-Growth Region (c) Grain-Refined Region (d) Base Metal.

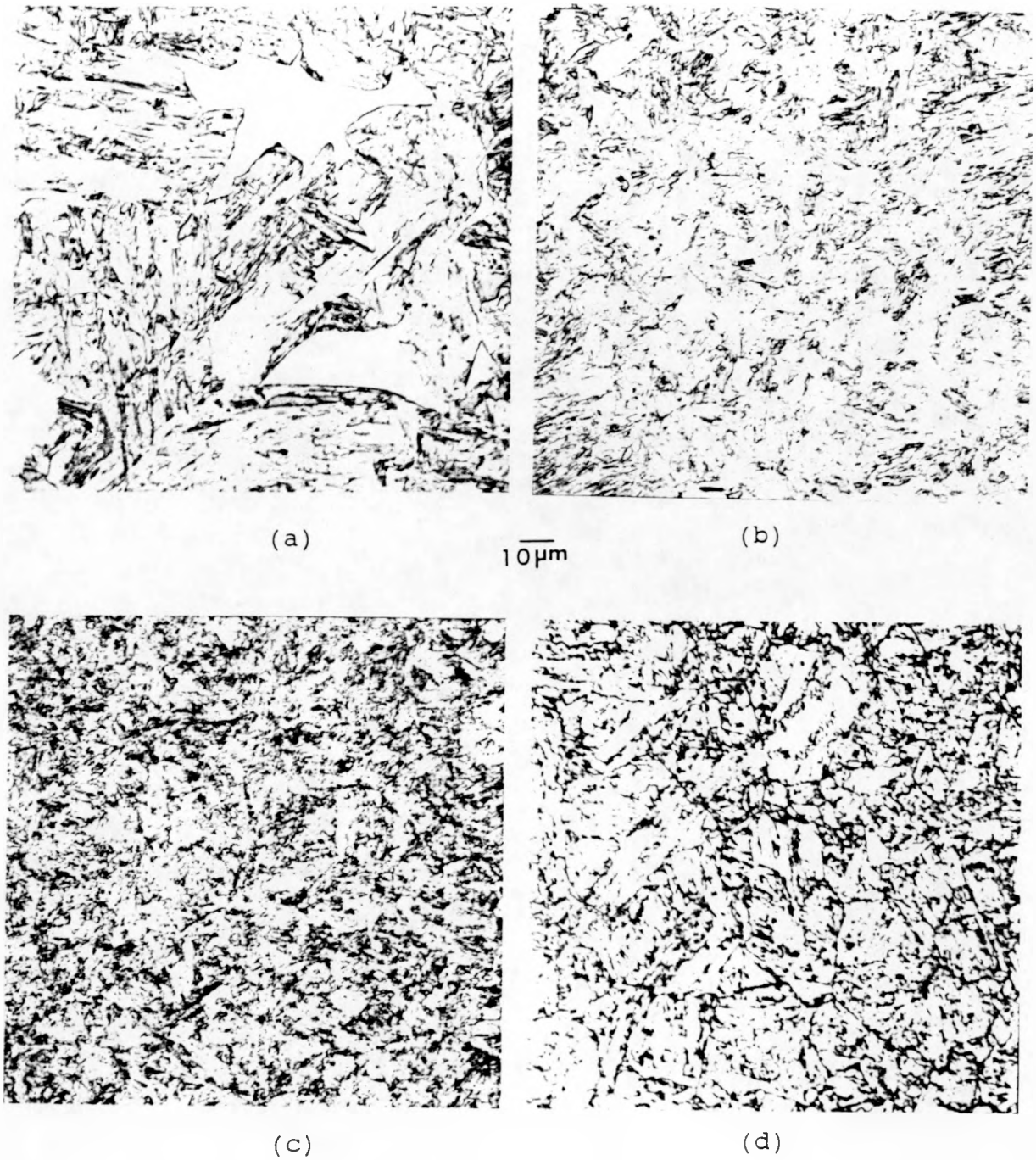

Figure 18. Optical Microstructure of 9 Cr-2WV Steel:
(a) Fusion Zone (b) Grain-Growth Region
(c) Grain-Refined Region (d) Base Metal.

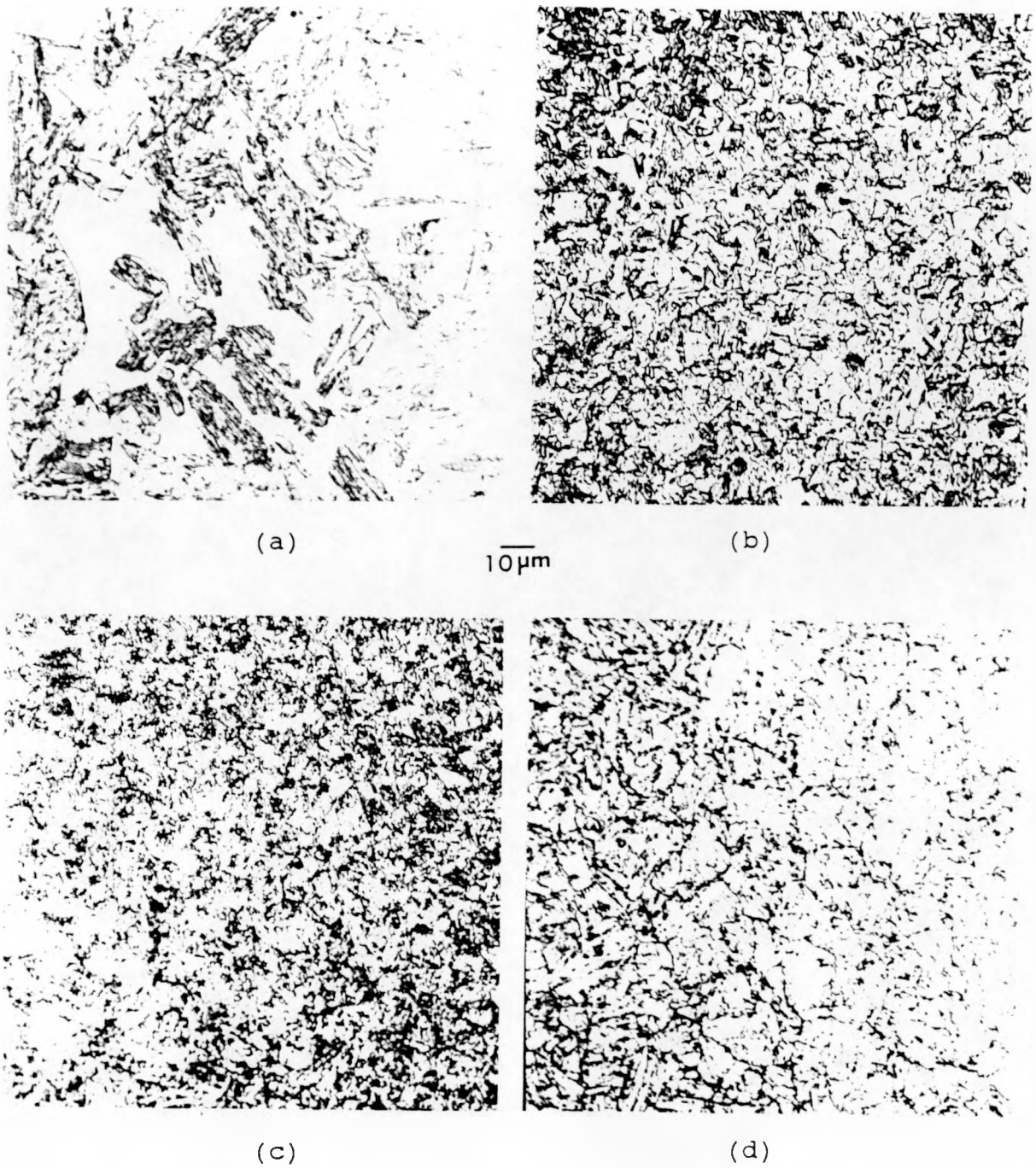

Figure 19. Optical Microstructure of 9 Cr-2WVTa Steel: (a) Fusion Zone (b) Grain-Growth Region (c) Grain-Refined Region (d) Base Metal.

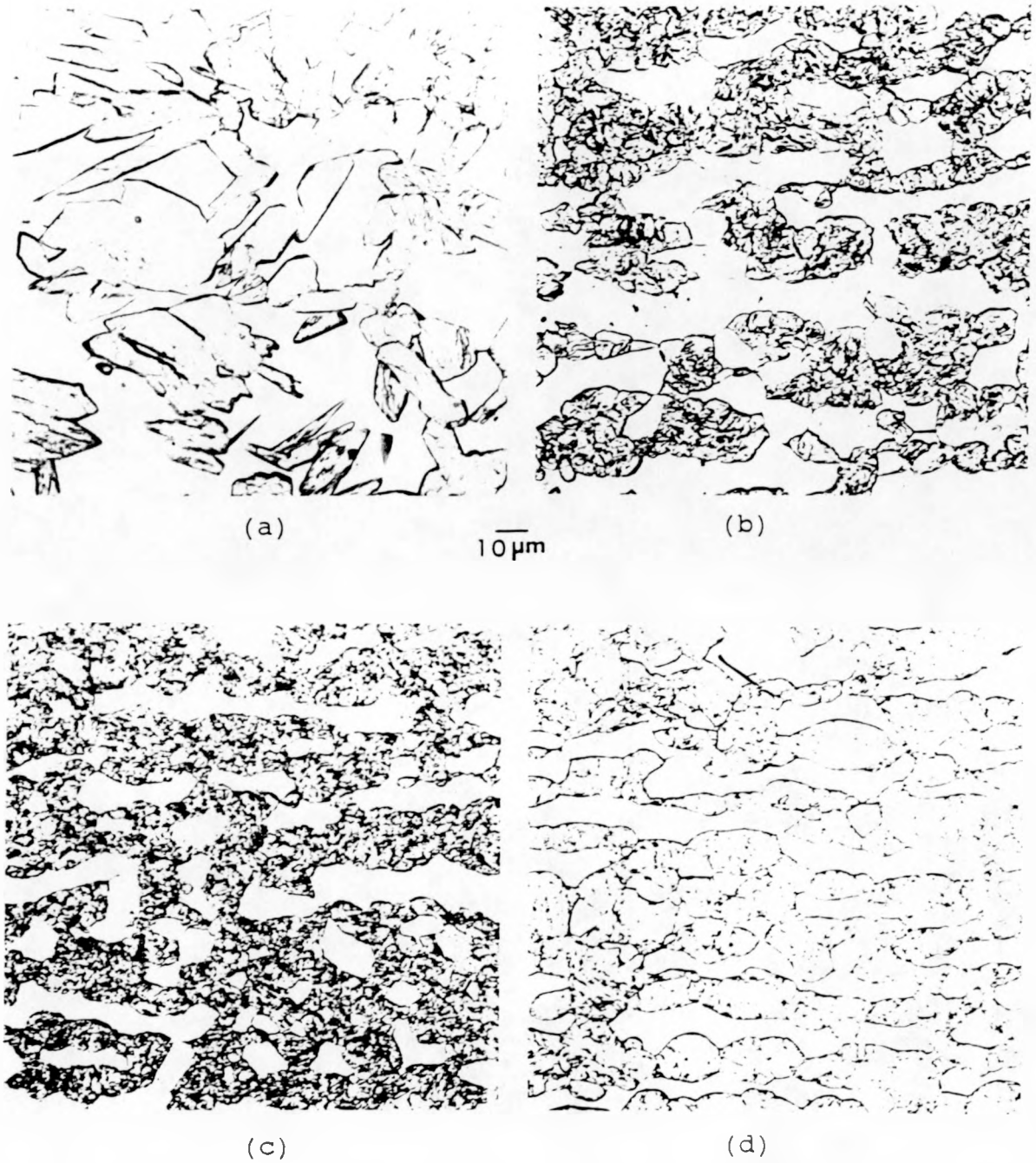

Figure 20. Optical Microstructure of 12 Cr-2WV Steel: (a) Fusion Zone (b) Grain-Growth Region (c) Grain-Refined Region (d) Base Metal.

Table 8. Microstructure of Low Activation Ferritic Steels.

2 1/4 Cr-V	8-12% polygonal ferrite + bainite
2 1/4 Cr-1WV	5-10% polygonal ferrite + bainite
2 1/4 Cr-2W	fully bainite structure
2 1/4 Cr-2Wv	3-8% polygonal ferrite + bainite
5 Cr-2WV	fully martensite structure
9 Cr-2WV	fully martensite structure
9 Cr-2WVTa	fully martensite structure
12 Cr-2WV	12-17% δ-ferrite + martensite

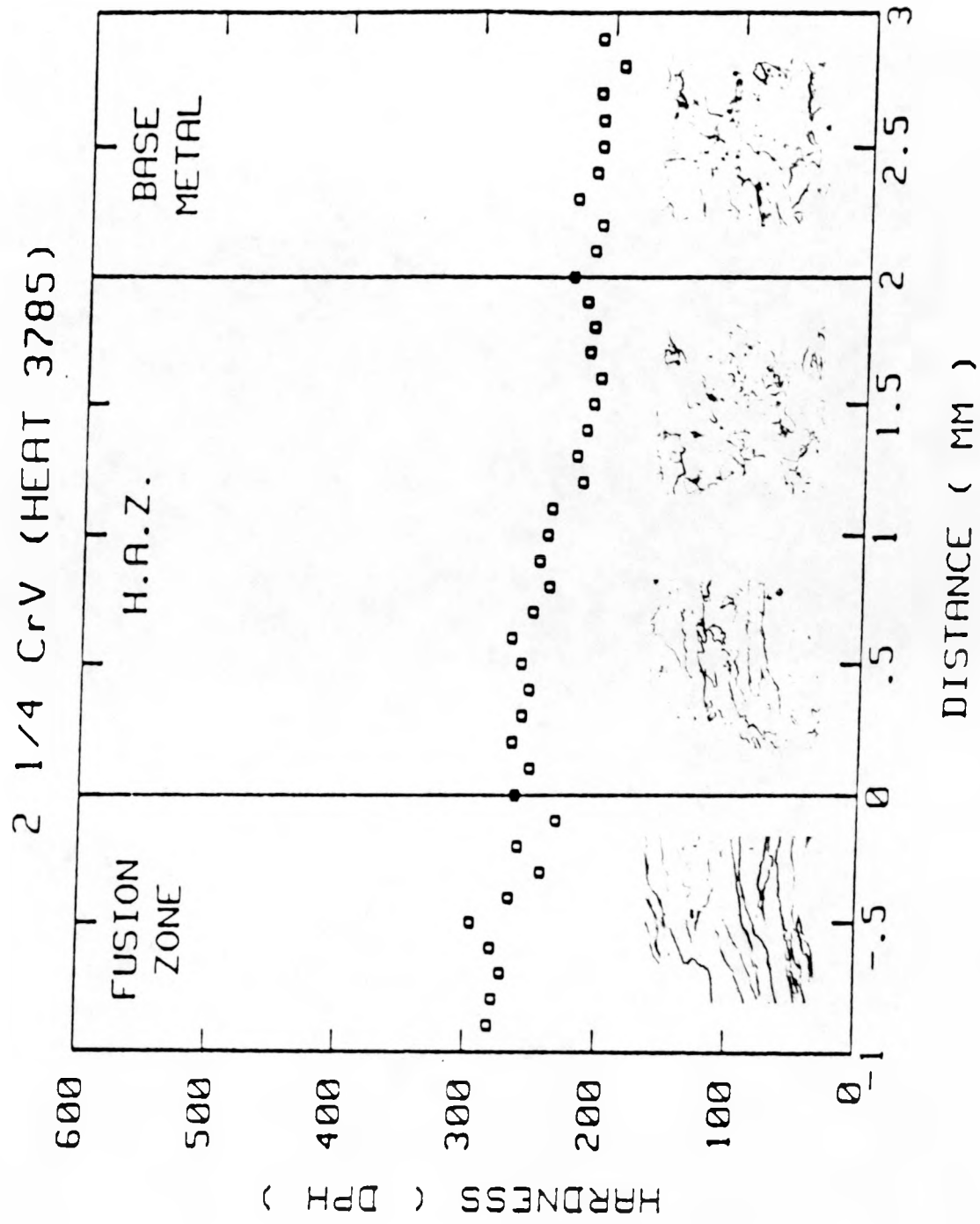

Figure 21. Diamond Pyramid Microhardness Measurements across the Weld of 2 1/4 CrV Steel with corresponding Microstructures.

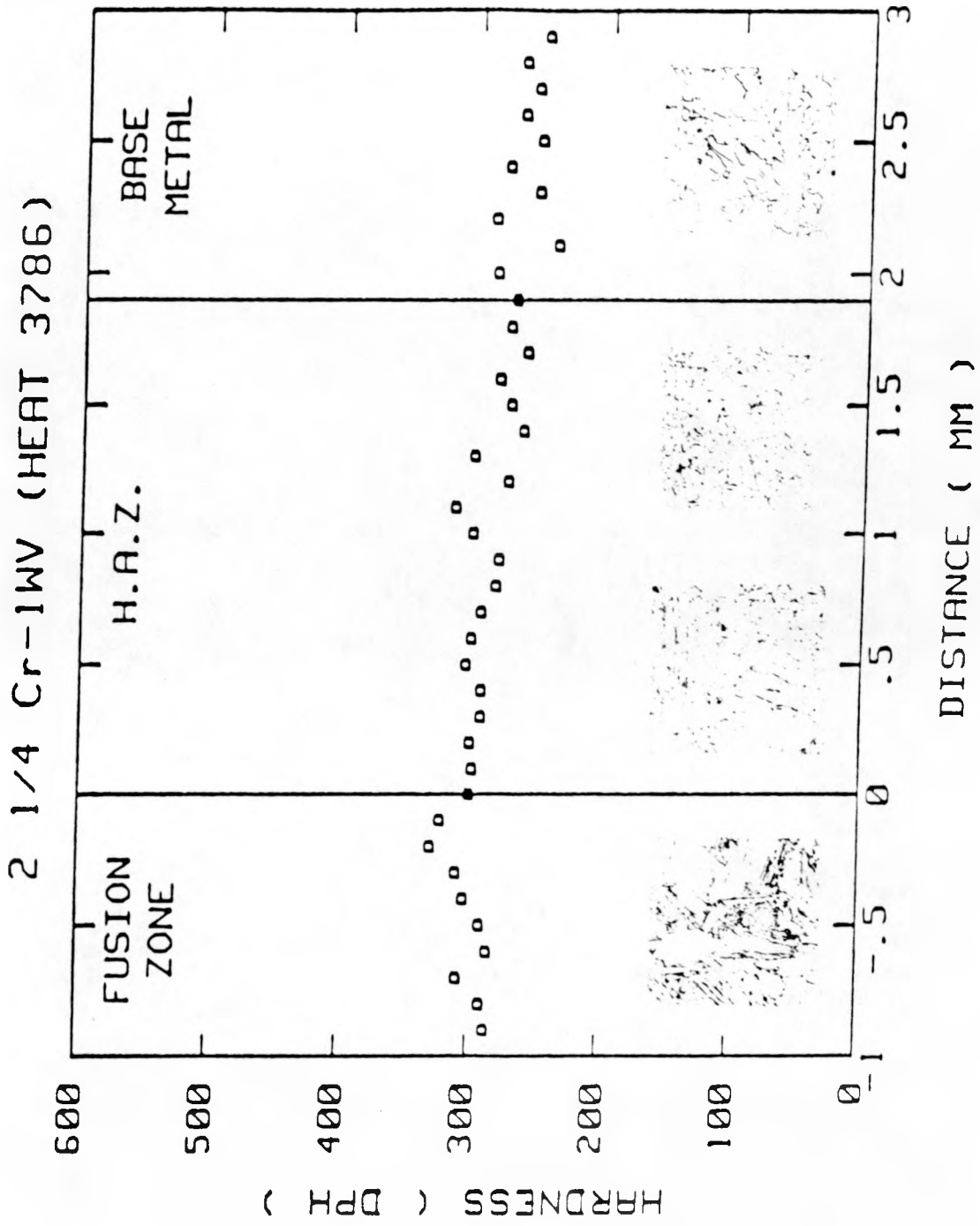

Figure 22. Diamond Pyramid Microhardness Measurements across the Weld of 2 1/4 Cr-1WV Steel with corresponding Microstructures.

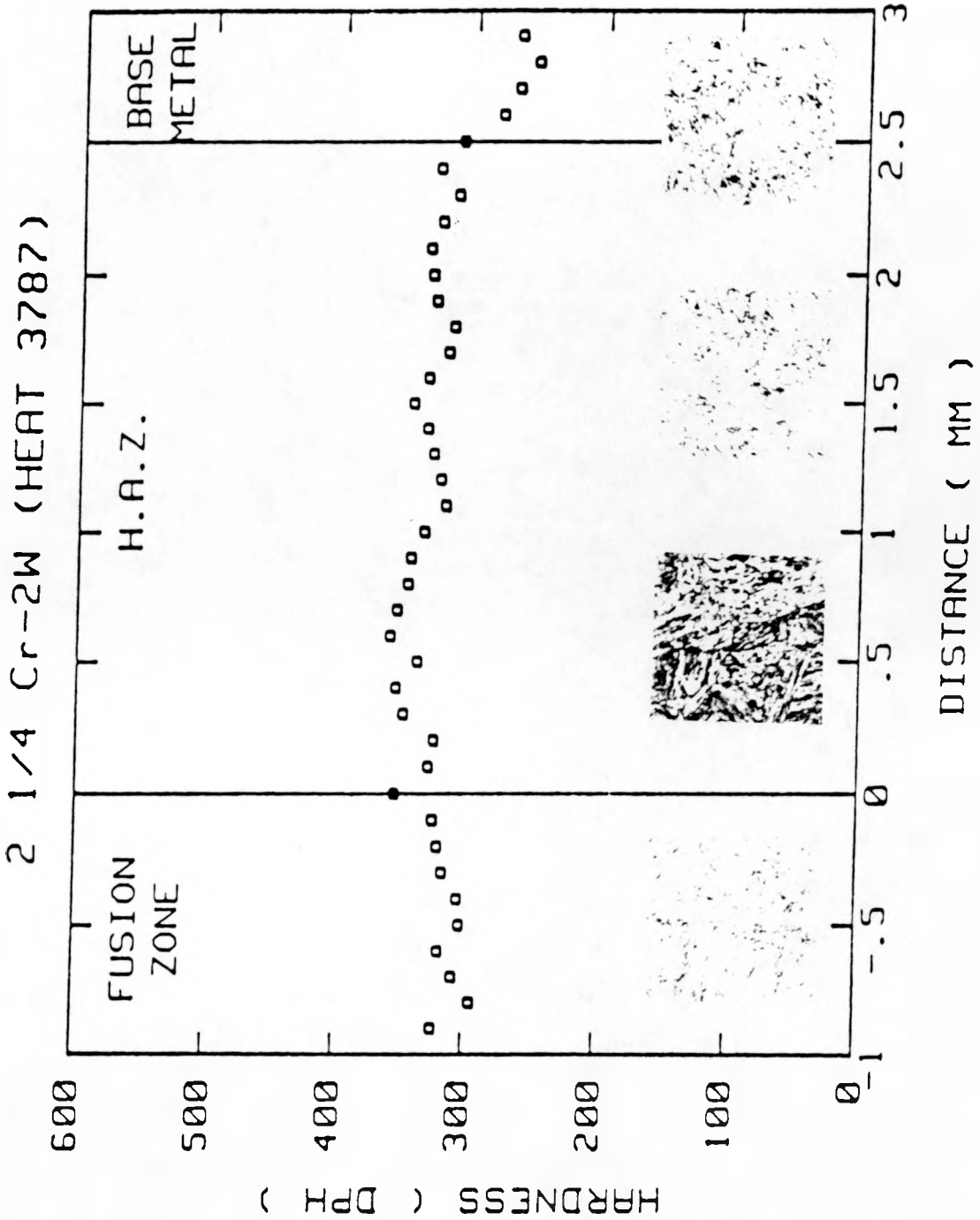

Figure 23. Diamond Pyramid Microhardness Measurements across the Weld of 2 1/4 Cr-2W Steel with corresponding Microstructures.

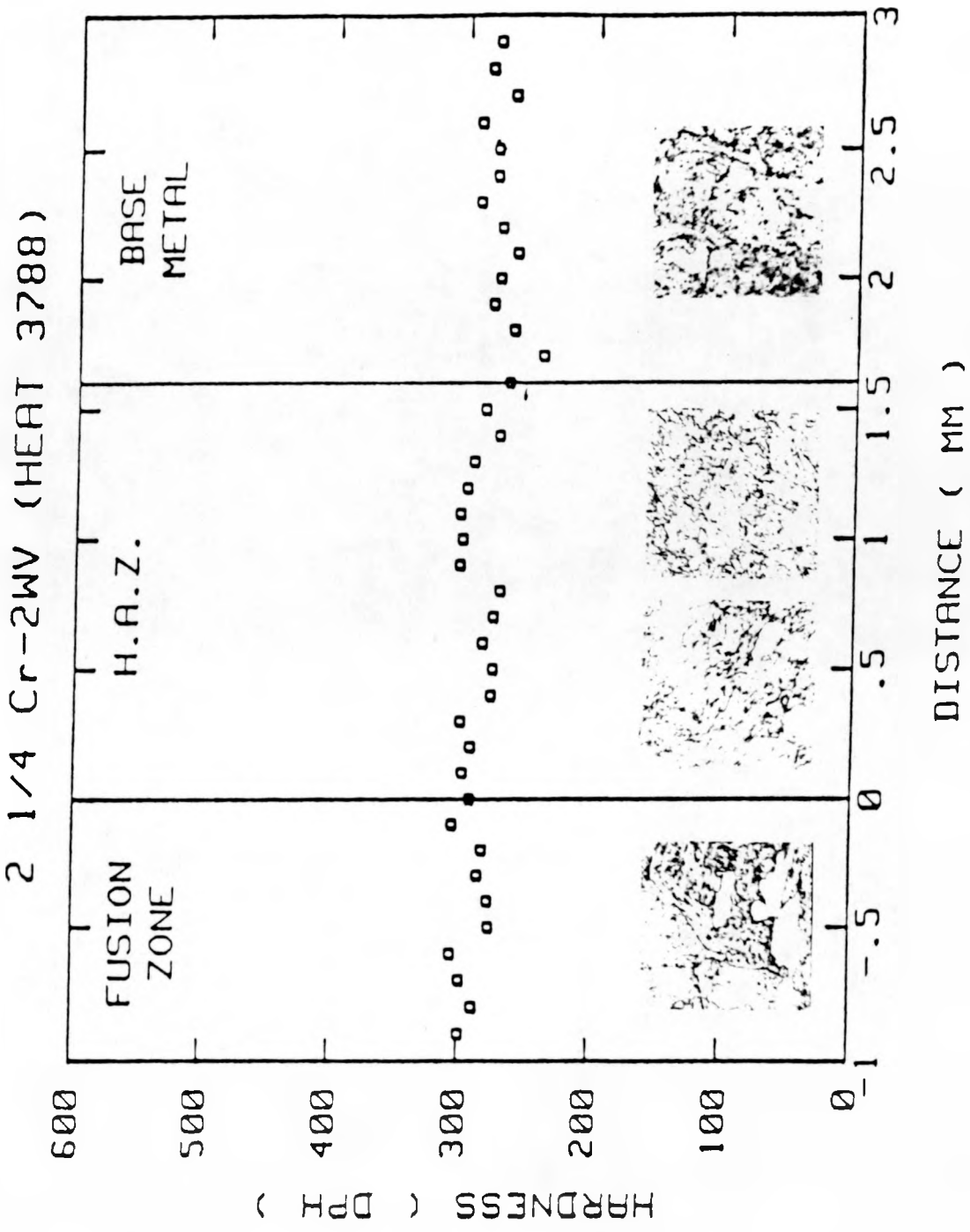

Figure 24. Diamond Pyramid Microhardness Measurements across the Weld of 2 1/4 Cr-2WV Steel with corresponding Microstructures.

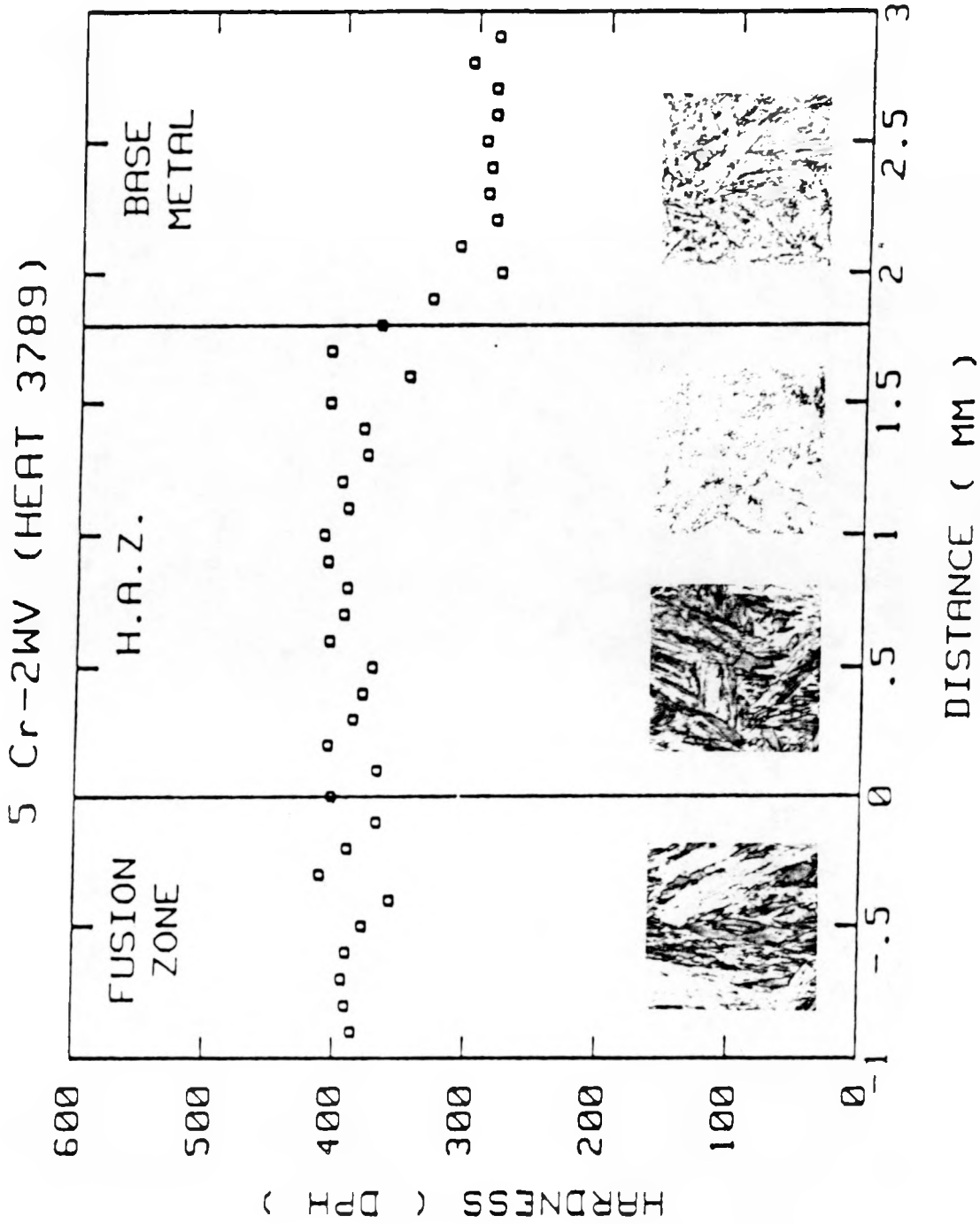

Figure 25. Diamond Pyramid Microhardness Measurements across the Weld of 5 Cr-2WV Steel with corresponding Microstructures.

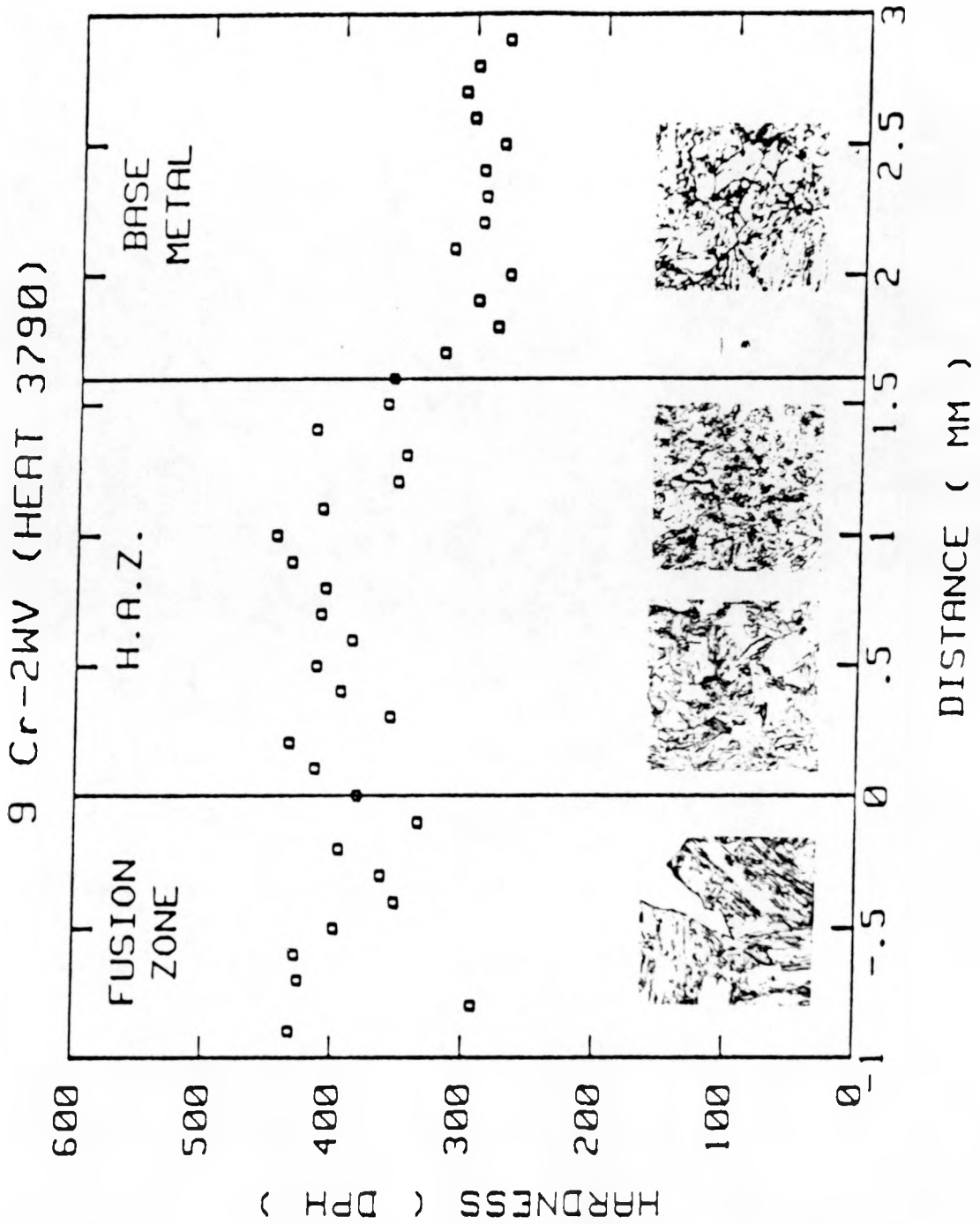

Figure 26. Diamond Pyramid Microhardness Measurements across the Weld of 9 Cr-2WV Steel with corresponding Microstructures.

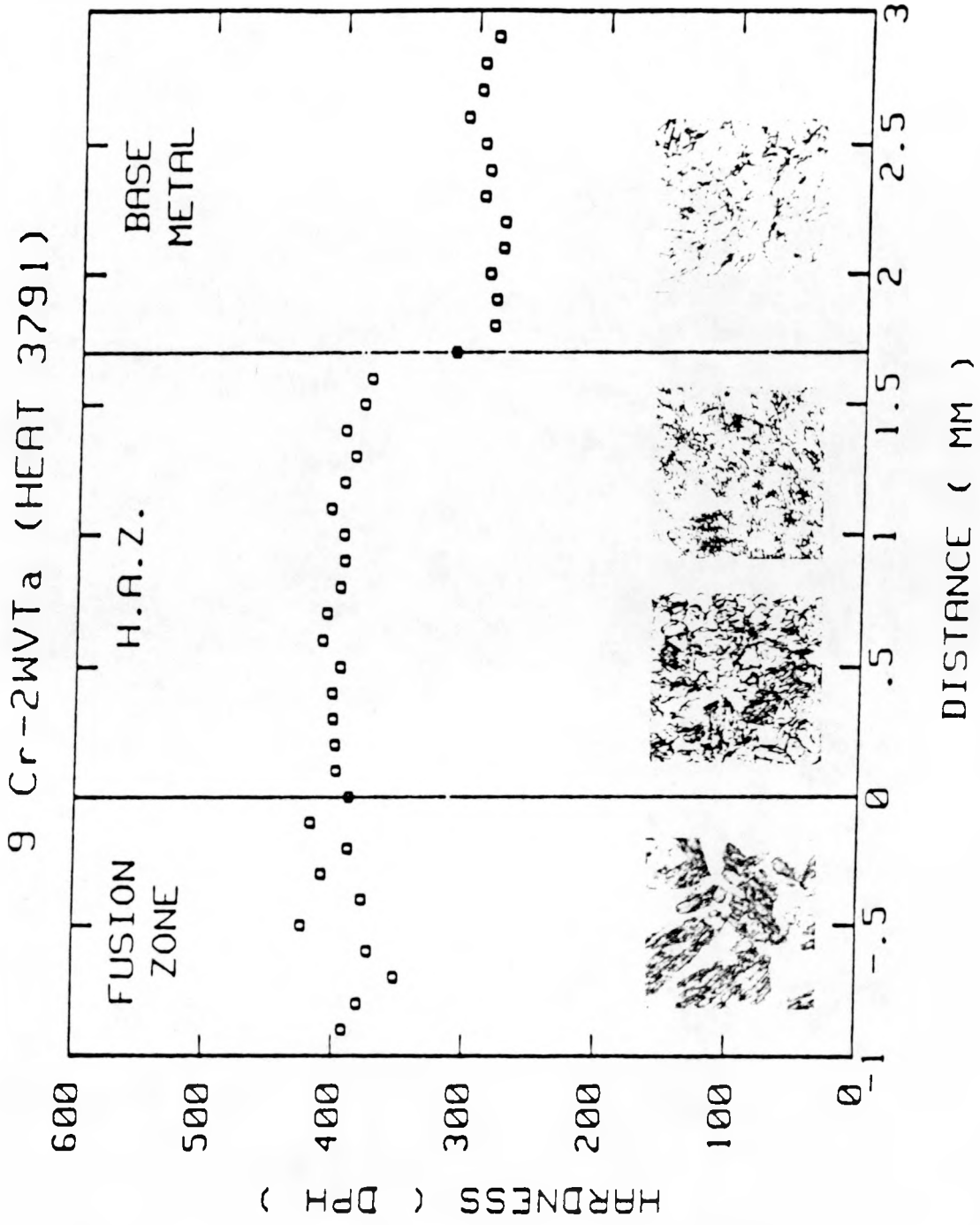

Figure 27. Diamond Pyramid Microhardness Measurements across the Weld of 9 Cr-2WVTa Steel with corresponding Microstructures.

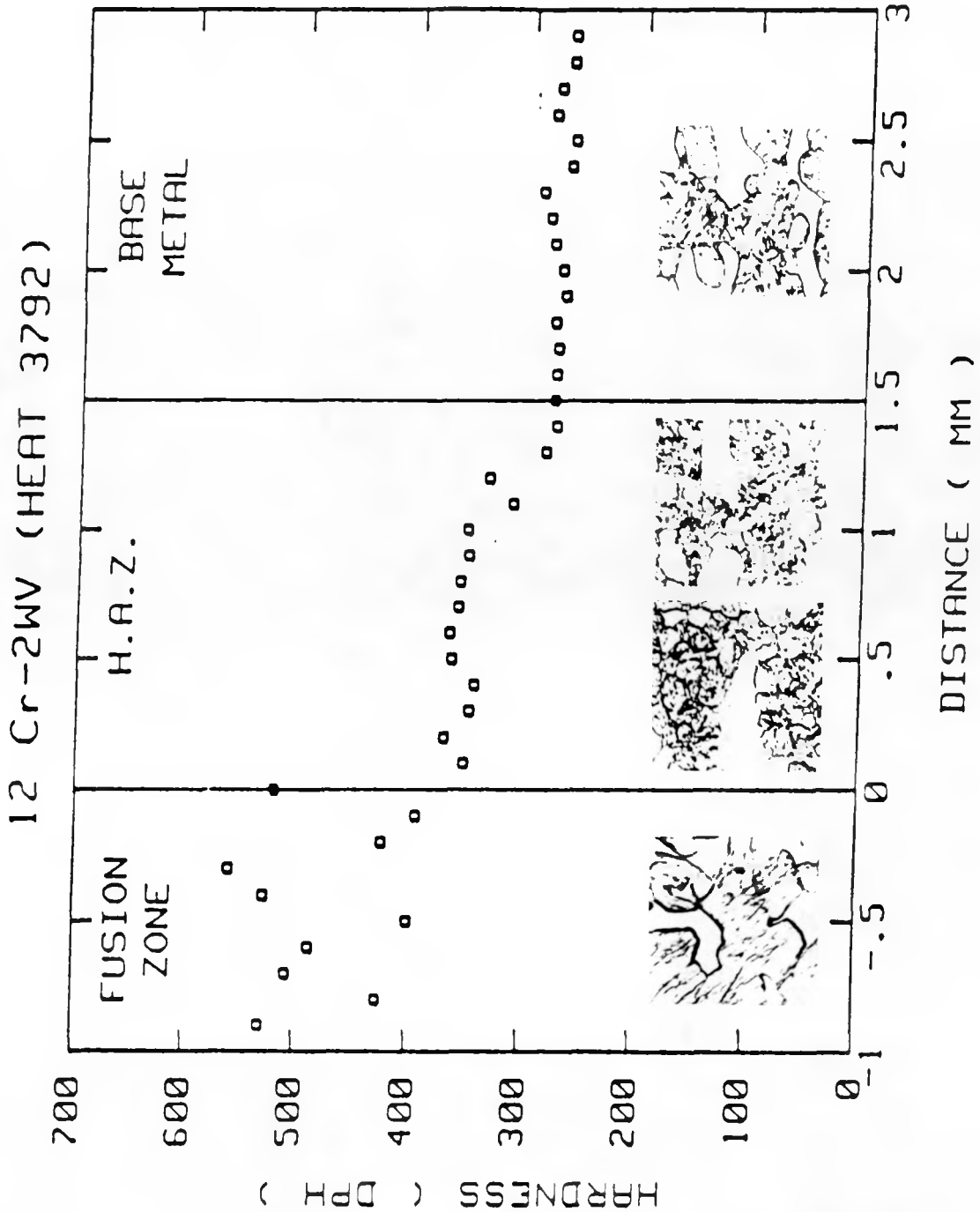

Figure 28. Diamond Pyramid Microhardness Measurements across the Weld of 12 Cr-2WV Steel with corresponding Microstructures.

averaged within a given region to obtain an overall average value. Table 9 lists the overall average values of DPH microhardness in different regions for the as-welded low activation ferritic steels.

In 2 1/4 Cr steel base metals, the highest hardness is found in 2 1/4 Cr-2WV steel, regardless of tempering condition. Without tungsten addition, the 2 1/4 Cr-V steel is the softest of all the low activation steels. With 1% tungsten addition, a significant increase of hardness is observed in the 2 1/4 Cr-1WV steel. A comparable hardness with 2 1/4 Cr-1WV is obtained for 2 1/4 Cr-2W steels in the quenched and tempered conditions. Nevertheless, the highest hardness is found in 2 1/4 Cr-2W steel in both the fusion and heat-affected zones after welding while 2 1/4 Cr-V steel still remains the same with the lowest hardness. A slight increase of hardness in both the fusion and heat-affected zones is found for all 2 1/4 Cr steels compared to that of the base metal, but a greater variation is observed in the 2 1/4 Cr-2W steel.

Microhardness is equivalent for all 5-12% Cr steels in the base metal and is greater than those of 2 1/4 Cr steels. Since 12 Cr-2WV steel contains 12-17% δ-ferrite, a lower hardness is observed compared to 5 and 9% Cr steels which are fully martensitic. Hardness is significantly increased in the fusion and heat-affected zones after GTA welding

Table 9. Measurements of Diamond Pyramid Microhardness for Low Activation Ferritic Steels.

Heat#		3785	3786	3787	3788	3789	3790	3791	3792
F.Z.	Ave.	268	295	327	307	388	381	390	480
	Max.	310	335	364	326	432	442	513	633
	Min.	212	280	298	275	340	330	212	236
HAZ	Ave.	237	288	333	295	391	398	398	356
	Max.	273	318	365	313	422	452	466	640
	Min.	205	264	306	265	349	345	344	291
B.M.	Ave.	209	255	264	273	295	293	291	280
	Max.	222	293	289	298	332	328	332	322
	Min.	185	232	230	233	268	262	259	241

compared to the base metal for 5-12% Cr steels. The average hardness is approximately the same in the fusion and HAZ for 5 and 9% Cr steels while the 12% Cr steel shows a dramatic drop from fusion zone to HAZ. Large scatter of microhardness in the fusion zone is observed for the 12% Cr steel.

Weld Bend Test

The initial three point bend test and the final 180° bend test were conducted on all welds. Experimental results are shown in Table 10. The 2 1/4 and 5% Cr steels exhibit adequate toughness in both initial and final bending and the results are satisfactory. The 9% Cr steels show adequate ductility in initial bending but fail at the fusion zone during final bending. As expected, the 12% Cr steel has poor properties in weld bend response. All 12 Cr-2WV steel samples failed at the fusion zone during either the initial three point bend or the final 180° bend. Figure 29 shows the load-deflection curve for the 12 Cr-2WV steel which failed in the initial three point bend. The material failed with a deflection range between 1.6 to 2.0 mm. This result suggests that the toughness and ductility is low for the 12 Cr-2WV steel weld.

The fracture surface was examined using a scanning electron microscope to investigate the fracture mechanism. Brittle failure is observed in the 9-12% Cr steel fracture surfaces. Figures 30-31 show the SEM fracture surface

Table 10. Results of Weld-Bend Test for Low Activation Ferritic Steels.

Alloy	Result
2 1/4 Cr-V	satisfactory
2 1/4 Cr-1WV	satisfactory
2 1/4 Cr-2W	satisfactory
2 1/4 Cr-2WV	satisfactory
5 Cr-2WV	satisfactory
9 Cr-2WV	failed at fusion zone
9 Cr-2WVTa	failed at fusion zone
12 Cr-2WV	failed at fusion zone

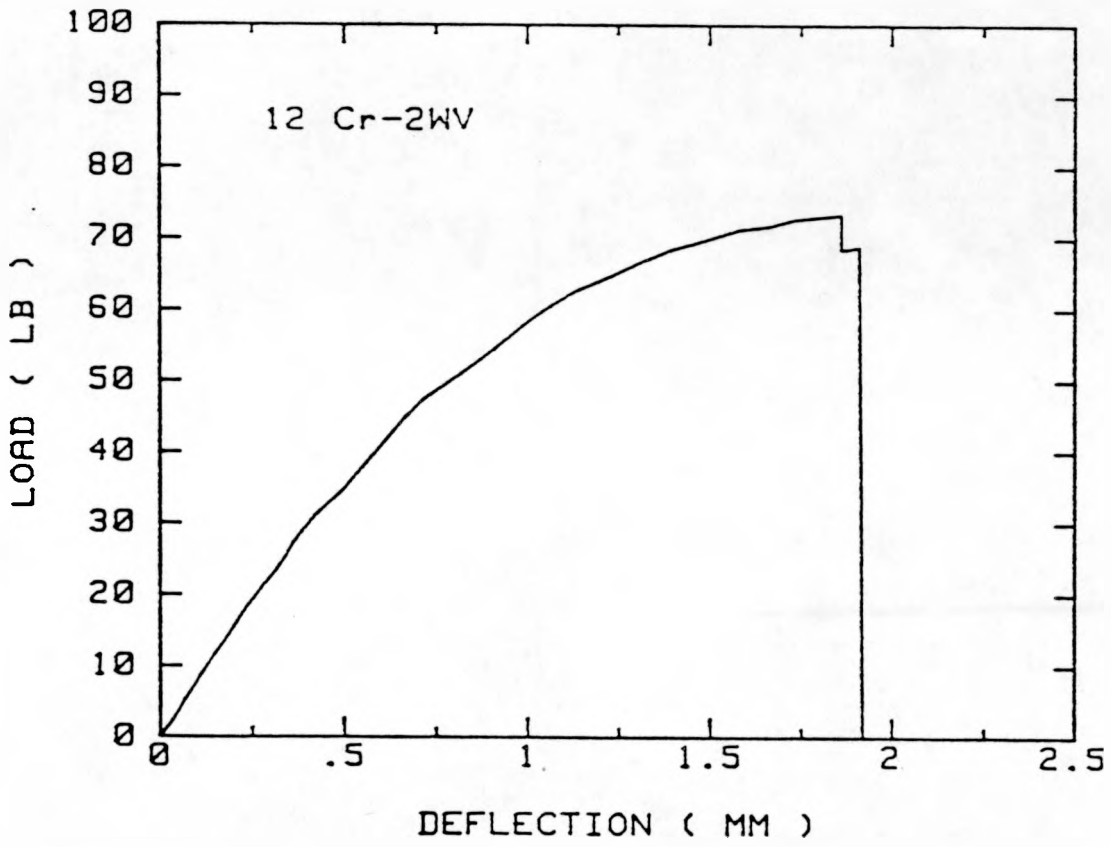

Figure 29. Load-Deflection Curve for the 12 Cr-2WV Steel during Three Point Bending.

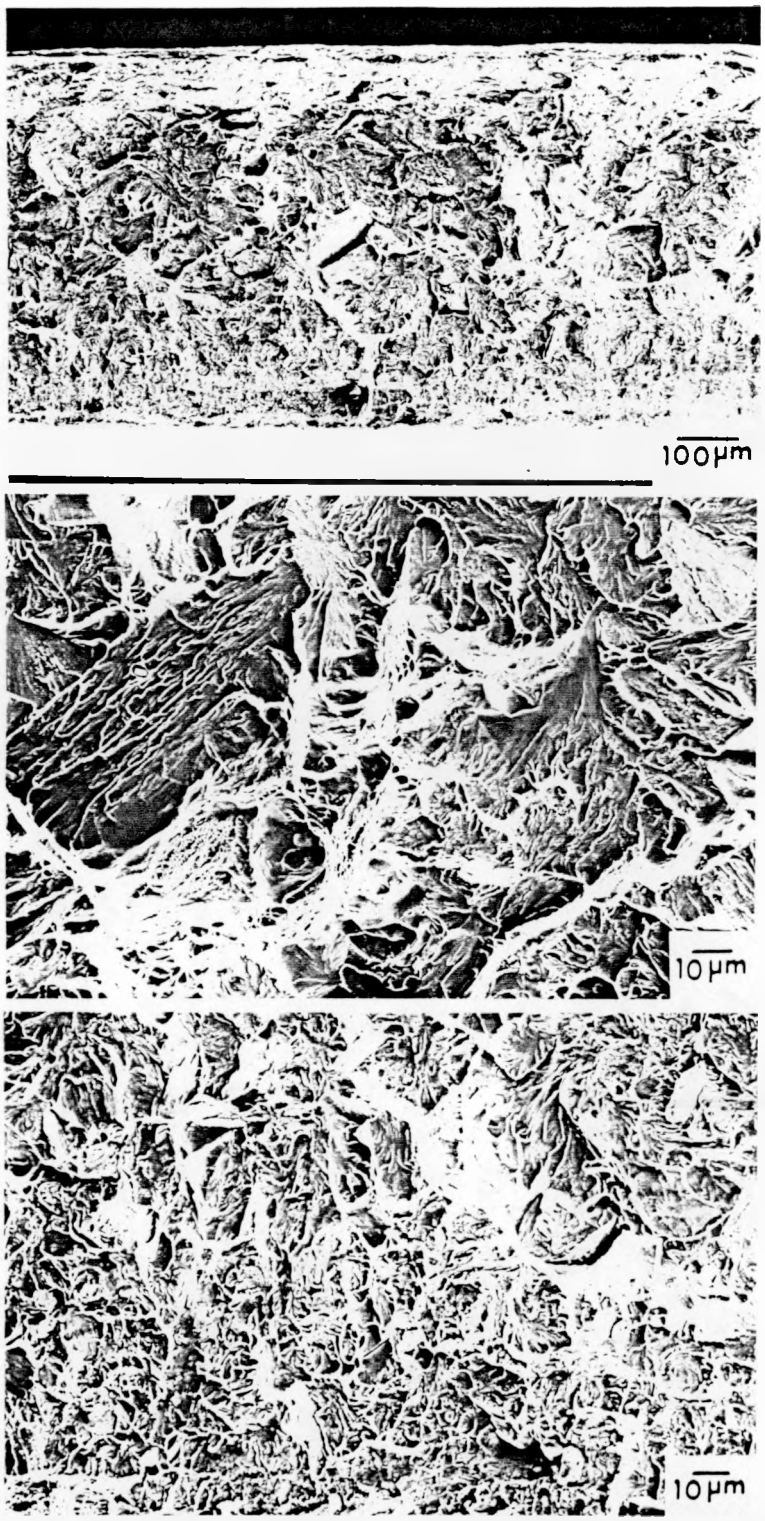

Figure 30. SEM Photographs for Fracture Surface of 9 Cr-2WV Steel after Final Bending: (a) Total Section (b) Center Coarser Grain Structure Region (c) Finer Grain Structure Region.

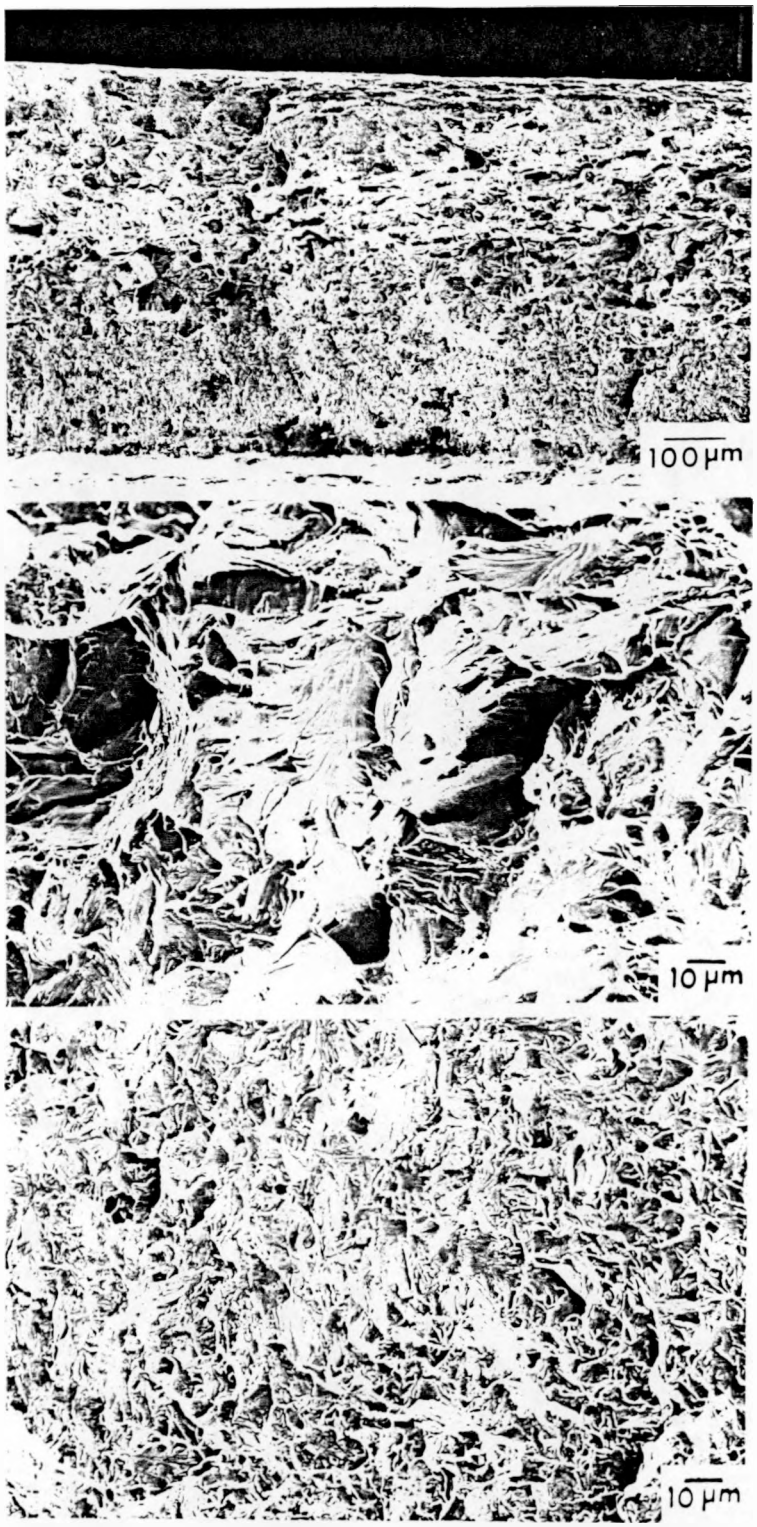

Figure 31. SEM Photographs for Fracture Surface of 9 Cr-2WVTa Steel after Final Bending: (a) Total Section (b) Center Coarser Grain Structure Region (c) Finer Grain Structure Region.

photographs for the 9% Cr steels. A finer grain structure is observed on the fracture surfaces of these steels. Both 9% Cr steels are dominated by brittle cleavage fracture with a small amount of dimple rupture at the rim around the fracture facets. Different modes of fracture are present in the fracture surfaces of the 12 Cr-2WV steel, as shown in Figure 32. At the center of the cross-section, transgranular brittle fracture is found while a mixture of transgranular and intergranular fracture is observed in the portion near the surface. A finer grain structure is also observed in the region next to the surface where a mixture mode of fracture occurred.

Tensile Tests

Both control and welded specimens were tested at room temperature at a strain rate of 6.67×10^{-4} sec^{-1}. Test results are listed in Table 11. The control specimens were tested along the rolling direction in the quenched and tempered condition. The as-welded tensile test was conducted in the loading direction perpendicular to the weld.

As shown in the results, 2 1/4 Cr-2WV steel has both the highest ultimate tensile strength and 0.2% offset yield stress of the 2 1/4% Cr steels for both control and as welded conditions. The lowest value of strength was again found in 2 1/4 Cr-2W. This is consistent with the microhardness measurement finding. The 2 1/4 Cr-1WV steel

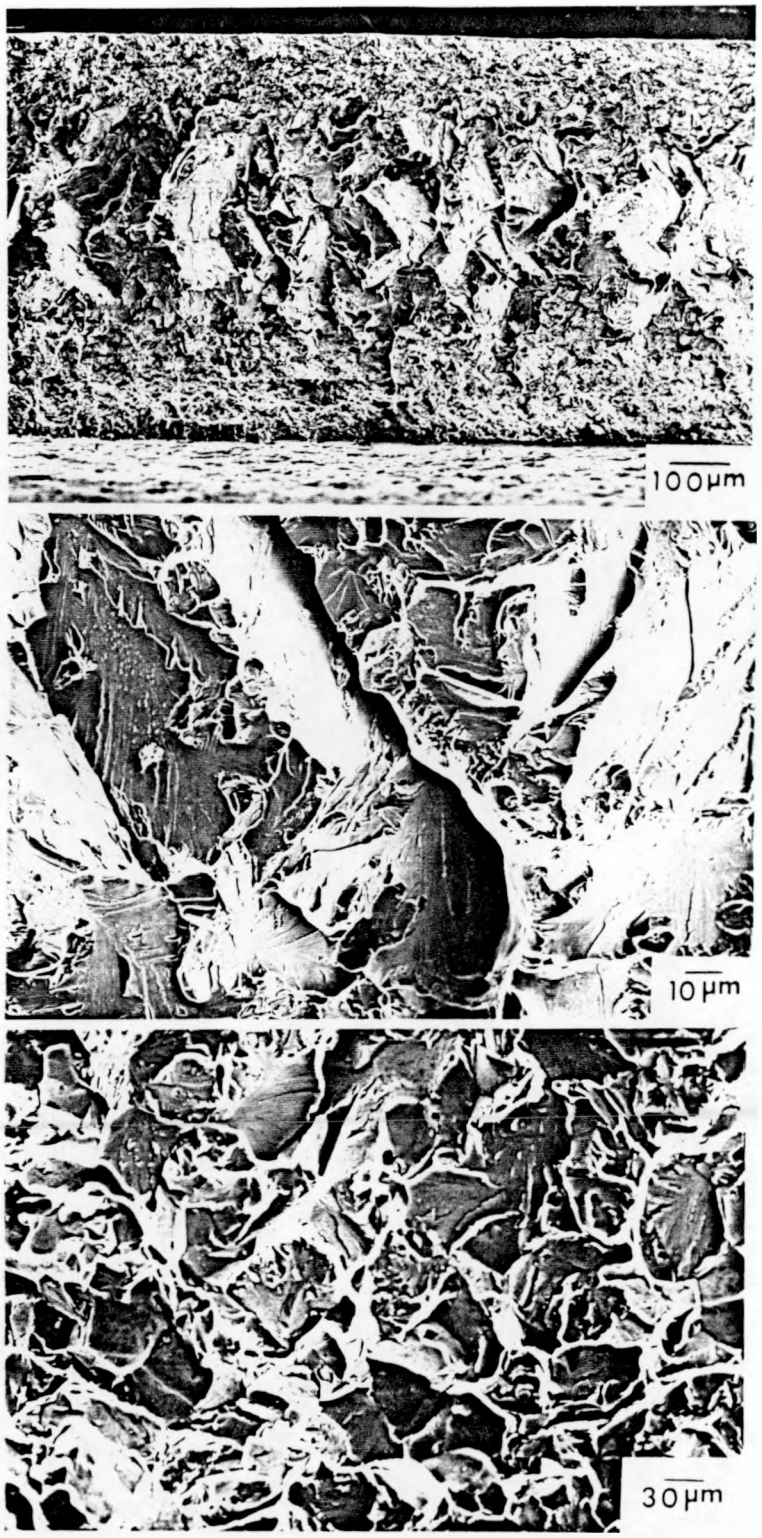

Figure 32. SEM Photographs for Fracture Surface of 12 Cr-2WV Steel after Final Bending: (a) Total Section (b) Center Coarser Grain Structure Region (c) Finer Grain Structure Region.

Table 11. Results of Room Temperature Tensile Test for Low Activation Ferritic Steels.

Steel		Strength (MPa) UTS	0.2% YS	Elongation (%) Uniform	Total
2 1/4Cr-V	control	516	428	7.2	18.0
	weld	443	326	6.5	15.0
2 1/4Cr-1WV	control	719	550	7.2	14.5
	weld	686	524	5.8	9.8
2 1/4Cr-2W	control	441	368	7.0	17.8
	weld	403	330	6.9	17.6
2 1/4Cr-2WV	control	727	588	6.6	12.4
	weld	719	567	5.7	9.4
5Cr-2WV	control	806	535	7.1	13.5
	weld	783	526	5.4	8.8
9Cr-2WV	control	842	595	7.2	12.2
	weld	786	572	5.7	10.5
9Cr-2WVTa	control	874	615	8.1	13.6
	weld	864	586	6.7	11.4
12Cr-2WV	control	832	578	9.4	13.2
	weld	802	556	6.4	11.2

shows a slightly lower strength than 2 1/4 Cr-2WV but a much greater strength than 2 1/4 Cr-V steel. To quantify ductility, the uniform elongation was used instead of the total elongation. Highly localized deformation and stretching is often observed after a major crack initiates. The highest uniform elongation is found in 2 1/4 Cr-V steel while 2 1/4 Cr-2WV steel appears to have the lowest ductility of the 2 1/4% Cr steels.

The 9 Cr-2WVTa steel has the highest tensile strength of all heats for both the control and the welded conditions and possesses a relatively high uniform elongation. The 5 Cr-2WV steel shows the lowest values in both strength and elongation for the 5-12% Cr steels. Even though the 12 Cr-2WV steel has slightly lower strength than the 9 Cr-2WV steels, it shows the highest ductility in uniform elongation of the 5-12% Cr steels.

It is readily found that the mechanical properties of these low activation ferritic steels degrade after gas tungsten arc welding. The area under the stress-strain curve, referred to as toughness, also decreases for all heats while the Young's modulus remains the same.

V. DISCUSSION

Welding Feasibility

Overall weld strength depends on the level of properties developed in each of the zones throughout the weld. In most fusion welds, the process results in steep temperature gradients. The material experiences rapid heating and cooling which renders the structure complex and nonequilibrium in nature. Experimental results show that the welds in all steels tested are sound and free of defects. The low carbon content in all steels tested contributes to this excellent weldability.

The weldability of steels is generally expressed in terms of carbon-equivalent [40].

$$C_{eq} = C + \frac{Si}{24} + \frac{Mn}{6} + \frac{Ni}{40} + \frac{Cr}{5} + \frac{Mo}{4} + \frac{V}{14}$$

This is an indication of the probable transformation that will occur in the heat-affected zone. Steels with a higher carbon-equivalent will have greater hardenability and therefore be more susceptible to heat-affected zone cracking due to martensitic transformations. Results from GTA welding are satisfactory for all steels in this study, especially for the 12 Cr-2WV steel. The commercial 12 Cr-Mo

steel cracks extensively in the heat-affected zone when no preheating is provided, whereas, 12 Cr-2WV steel is free of cracks. This low susceptibility to HAZ cracking is hypothesized to be a result of the delta ferrite present in the microstructure.

Alloying Effect on Microstructure

Optical microscopy examinations show that the microstructure of low activation ferritic steels varied with chemical composition. The 2 1/4 Cr steels are typically composed of a bainitic structure. In a comparing of these steels, alloying additions were found to have a significant effect on the quenched and tempered microstructure. Without tungsten additions, 2 1/4 Cr-V steel contains 8-12% proeutectoid polygonal ferrite. As tungsten is added, 2 1/4 Cr-1WV has 5-10% polygonal ferrite and 3-8% ferrite is observed in the 2 1/4 Cr-2WV steel. No polygonal ferrite was observed in the 2 1/4 Cr-2W steel. This result suggests that the addition of tungsten increases the hardenability of 2 1/4% Cr steels.

It is possible to form complete bainite when 2% tungsten is added into the steels. Nevertheless, it was experimentally found that the 2 1/4 Cr-2WV steel contained proeutectoid ferrite. This phenomenon probably resulted from vanadium carbides present in the steel not completely dissolving during austenitization. Vanadium carbide ties up

carbon that would normally be in solution and hence decreases the hardenability.

A martensitic structure is observed in the 5-12% Cr steels. This result implies that chromium effectively increases the hardenability to a level that is great enough to form martensite instead of bainite. The 5-9% Cr steels are fully martensite whereas the 12 Cr-2WV steel contains 12-17% δ-ferrite. The reason for the ferrite presence is insufficient austenite-stabilizing elements such as carbon, nickel and manganese. Both ferrite and austenite exist in the microstructure at the austenitizing temperature due to insufficient austenite forming elements. Austenite transforms to martensite upon cooling whereas ferrite remains. This ferrite is referred to as delta-ferrite. Unfortunately, carbon is restricted to 0.1% to ensure sound welding while nickel is not favored from a low activation point of view. Therefore, the composition modification with manganese may be the best choice to promote a fully martensitic structure in the 12% Cr steel. On the other hand, it is known that chromium and tungsten, ferrite-stabilizers, tend to promote delta-ferrite formation.

In 9% Cr steels, a finer martensite structure is found than in the 9 Cr-2WVTa steel. This is attributed to the addition of tantalum which considerably decreases the prior austenite grain size. Tantalum behaves similar to niobium in the commercial 9 Cr-Mo steel. Tantalum exists in 9 Cr-

2WVTa steel in the form of carbide precipitates with a high melting point. During the austenitization process, tantalum carbide precipitates dissolve slowly or even remain in the solid form and act as pinning particles to confine grain growth. Therefore, a finer structure is obtained after solidification.

The as-welded microstructure consists of four distinct regions (fusion zone, grain-growth and grain-refined regions in HAZ, and base metal) for all heats. The previous discussion of the microstructure in quenched and tempered condition is exactly identical to the case of the base metal. All the 2 1/4% Cr steels, except the 2 1/4 Cr-2W steel, consist of bainite and ferrite in both fusion and heat-affected zones due to vanadium carbides present as described above. The 2 1/4 Cr-2W steel remains fully bainitic in both zones.

Although the 5 and 9% Cr steels are fully martensite under quenched and tempered conditions, a mixture of martensite and ferrite is present in both the fusion and heat-affected zones. Lesser amounts of ferrite is found in the 5% Cr steel. Steels with lower chromium content Cr is a ferrite stabilizer possess a lower austenite transformation temperature. As a result, the 5% Cr steel will have a lesser amount of ferrite fraction compared to 9% Cr steels at the same temperature (higher than the austenite transformation temperature). Consequently, less amount of

ferrite is found after solidification. Both fusion and heat-affected zones are mixed with martensite and delta ferrite for 12 Cr-2WV steel as in base metal due to insufficient austenite forming elements present in the steel.

Alloying Effect on Microhardness

In order to evaluate the effect of tungsten and vanadium on hardenability, 2 1/4% Cr steels fusion zone and heat-affected zone microhardness were compared. The lowest hardness is found in 2 1/4 Cr-V steel. With 1% tungsten addition, a much higher hardness is obtained for 2 1/4 Cr-1WV steel. Microhardness slightly increases with increasing tungsten content up to 2% as in the 2 1/4 Cr-2WV steel. Without the vanadium addition, 2 1/4 Cr-2W has the highest hardness in 2 1/4% Cr steels. These results indicate that both tungsten and vanadium increase the hardenability for 2 1/4% Cr steel. Tungsten shows a greater effect than vanadium. The vanadium carbides which do not dissolve during austenitization will decrease the solution carbon concentration and hence the hardenability. Therefore, 2 1/4 Cr-2W steel is expected to have the highest hardenability and hardness.

Since martensite hardness is not sensitive to the cooling rate [41], a comparison can be made to investigate the effect of chromium on hardenability. It is obvious that chromium has a tremendous contribution on hardenability by

comparing all the steels. The higher the Cr content, the higher the hardness. The lower hardness in the heat-affected zone for 12 Cr-2WV steel compared to others is a result of the presence of delta ferrite. The scattering of microhardness at the fusion zone is also attributed to the ferrite presence. Tantalum additiond in the 9% Cr steels does not have much influence on the hardenability but does significantly reduce the grain size by the carbide precipitate pinning process.

The high microhardness present in the fusion and heat-affected zones is attributed to untempered martensite. A very high dislocation density is a result of nonequilibrium solidification during fast cooling from high temperatures. With tempering, dislocations are recovered which alleviates to an extent the hard and brittle nature. Different steels appear to have different responses to the tempering process when microhardness of the base metal is compared. The final properties depend on the carbide precipitation and time-temperature response during the tempering process. This dependence will not be discussed in this study. The data shown in Table 9 are for tempering condition at 700°C for one hour. The 2 1/4 Cr-V steel again has the lowest value but 2 1/4 Cr-2WV has a greater hardness than 2 1/4 Cr-2W steel. The 5-12% Cr steels show equivalent hardness.

Weld Bend Test

In order to evaluate the ductility and soundness of the weld, control materials were tested under quenched and tempered conditions. Results from the weld bend test show that all 2 1/4% Cr steels have excellent ductility in the welds. No failure was observed. The microstructure of these low chromium steels consists basically of a bainite structure which is characterized with high strength and excellent toughness. A similar result was obtained for the 5 Cr-2WV steel despite its martensite structure. It was found that the 5% Cr steel shows an intermediate toughness between 2 1/4 and 9% Cr content steels (impact tests as shown in Table 4). This is attributed to the medium hardenability of the 5% Cr steel.

Results are satisfactory in the initial three point bending test for both 9 Cr-2WV and 9 Cr-2WVTa steels. All welds have adequate ductility in this stage. Nevertheless, some specimens failed at either the fusion zone or the interface of the fusion and heat-affected zone during the final stage of the 180° bend test. This failure is inherent in welds of materials with a martensitic structure. The constituents in the fusion zone consist of untempered martensite and polygonal ferrite. The untempered martensite is hard and brittle in nature. The ductility is relatively low in the as-welded condition. Carbide precipitates will form when steels are subjected to the tempering process and

thus will toughen the material. Although the weld failed during final bending, ductility is acceptable for the 9% Cr steels.

Fusion zone failures were observed in all the 12% Cr steels. Some of the 12% Cr steels failed in the initial three point bend tests. The maximum deflection was only 2 mm when failure occurred. This indicates that poor ductility results in 12 Cr-2WV steel that is subjected to gas tungsten arc welding. Two reasons are responsible for the deterioration of ductility for the 12% Cr steel. First, the high Cr content effectively increases the hardenability. The weld is cooled at a very high cooling rate from the melting point. The untempered martensite is again hard and brittle and deformation is restricted. Second, the presence of delta ferrite reduces the toughness substantially [42]. Anderko, et al. also concluded that elements which suppressed the formation of delta ferrite produced lower DBTT than elements, such as Cr, that promote delta ferrite formation [43]. The nonuniformity in structure and strength often easily leads to crack formation.

Fracture Mechanisms

Fracture surfaces of the weld bend test specimens show that the steels are composed of a finer structure near the surfaces. The finer grain structure near the surface is probably due to the specimen preparation. Specimens were wrapped with zirconium foil and austenitized in argon atmosphere then quenched into water. The specimen surface contacted with water via the zirconium foil and hence is subjected to a higher cooling rate than the center. The fast cooling rate restricted grain growth at the surface while in the center grains grew to a larger extent.

Brittle fracture is predominant in the 9% Cr steels with a transgranular cleavage mode in both the coarse and the fine structure. Some dimple rupture can be seen near the rim of the brittle cleavage facets in both steel fracture surfaces. This dimple structure is referred to as the ductile fracture mode. This is probably where the soft ferrite phase is located. The brittle fracture mode in 12 Cr-2WV steel is attributed to its high hardenability and the present of delta ferrite as discussed above. This result is consistent with the microhardness results. However, the reason for a slight intergranular decohesive fracture mode in the finer grain structure region is not apparent. Several mechanisms can lead to this situation. For example, impurities (such as sulfur and phosphorus) may segregate along the grain boundaries and significantly reduce the

cohesive strength of the material at the boundaries and promote decohesive rupture.

Alloying Effect on Tensile Properties

The alloying elements are known to play an important role in the microstructure and microhardness as discussed above. Consequently, they significantly influence the tensile properties of these low activation steels.

Without vanadium additions, tempered 2 1/4 Cr-2W steel appears to have the lowest strength but possesses excellent ductility. Locally extensive deformation is observed during tensile tests after cracks initiate in the 2 1/4 Cr-2W steel as the data shows in total elongation. An analogous response to the alloying effect is found in steels when no tungsten is added. Tempered 2 1/4 Cr-V steel has a strength greater than 2 1/4 Cr-2W steel but much lower than the other heats. Extensive elongation is also observed for the 2 1/4-V steel. This difference in strength suggests the vanadium has a greater effect on improving the tensile properties.

Tensile property results indicate that a large additive effect occurred for steels containing tungsten and vanadium. The combined use of chromium and vanadium in these newly developed steels result in high tensile strength, accompanied by excellent ductility. The 2 1/4 Cr-1WV steel has a much greater tensile strength than both the 2 1/4 Cr-V and 2 1/4 Cr-2W steels but slightly lower than the 2 1/4 Cr-2WV steel. Observations reveal that coarser carbide

precipitates are found in 2 1/4 Cr-V steel and increases in tungsten content decreases the size of carbide precipitates [44]. This is attributed to the increase in hardenability with tungsten. The transformation temperature is effectively decreased by tungsten and therefore the finer precipitates. Finely dispersed precipitates significantly impede the dislocation motion and increase the strength. However, the addition of tungsten or vanadium alone does not give a satisfactory strength. Steel, 2 1/4 Cr-2W, with tungsten addition has a coarser carbide precipitate distribution than that of steels without tungsten, 2 1/4 Cr-V, or containing vanadium, 2 1/4 Cr-2WV. This explains why the lowest strength is found in 2 1/4 Cr-2W steel and shows the remarkable additive effect of Cr and V.

The effect of chromium content on the tensile properties can be obtained by comparing the steels containing 2% tungsten and 0.25% vanadium. The tensile test results show that strength increases with increasing chromium content. However, a different result is presented by Klueh, et al. They concluded that chromium had a nonlinear strengthening effect on these steels and showed a minimum strength in 5 Cr-2WV steel due to the coarser carbide distribution [45].

The lower strength in the 12 Cr-2WV steel is attributed to the large amount of delta ferrite present in the microstructure. The presence of delta ferrite increases the

nonuniformity of steel and hence the instability in deformation. However, the ductility remains adequate because of the soft ferrite. With tantalum additions, the grain size of 9 Cr-2WVTa is effectively reduced by the precipitate pinning process and strength, therefore, is increased.

VI. CONCLUSIONS

From the results and previous discussion in this study, conclusions are summarized as follows:

1. Sound autogenous welds can be achieved by conventional gas tungsten arc welding in 2 1/4 and 5% Cr low activation ferritic steels.
2. Post-weld heat treatment is necessary in the 9-12% Cr steels to restore the toughness especially for the 12% Cr steel.
3. Chromium, vanadium and tungsten additions strengthened all steels tested. V and W show significant effects.
4. Tantalum effectively refines the grain size and strengthens the steel.

BRAZING OF COPPER-ALUMINA ALLOYS

I. ABSTRACT

The GLIDCOP Al-15 alloy has been targeted for use in tokamak fusion reactors. This choose was made because of the alloy's ability to retain a cold worked structure at elevated temperatures and its high heat carrying capacity, and electrical conductivity. Specific uses of the alloy are as a structural material in diverter and limiter assemblies and as magnets. However, the successful use of this alloy depends on the ability to join the alloy during fabrication without destroying its properties. Thus, a brazing process that does not alter the alloy's structure or properties is highly desirable for the design of these devices and their successful application in tokamak reactors.

The development of an induction brazing process for GLIDCOP Al-15, a cold worked copper-0.15 aluminum alloy, will eliminate 3 major problems associated with furnace brazing of GLIDCOP Al-15:

1. Plating the joining surfaces prior to brazing if a material (braze alloy) is used.
2. Using an inert cover gas or a vacuum pump to prevent excessive oxidation.
3. Lowering of the yield and ultimate tensile strength by approximately 20% due to recovery of the matrix.

The objective of the research that is being conducted is the development of an induction brazing process for

GLIDCOP Al-15 using a silver-based brazing alloy. This objective centers on minimizing the time required at elevated temperatures during the brazing process in order to eliminate the problems of furnace brazing.

II. EXPERIMENTAL PROCEDURE

Brazed joints will be produced by using a 50 Kw induction furnace with an oval shaped helical coil. The samples will be electrically insulated from the coil by means of a quartz tube. Very fine copper wire is to be wound about the joint that is to be brazed to hold the 0.003" thick BAg-5 brazing alloy in place and to keep the two metal strips straight. A range of braze times and power settings for consistent brazing will be developed.

Microhardness measurements will be made both lengthwise and across the brazed section. Measurements will be made at a number of places in the brazed section and at 1 mm intervals from the brazed region into the base metal.

Rectangular strips of constant cross-sectional area are to be brazed and then machined into tensile specimens. A pin loaded single-lap shear test specimen (Figure 34) according to the AMERICAN WELDING SOCIETY STANDARD is to be used for evaluating the strength of brazed joints in shear. Additional mechanical testing will be done using miniature tensile specimens (Figure 34). Strain data for the miniature tensile specimens will be obtained using a LASERMIKE 162-100 Laser Scanner with a LASERMIKE 1010 Processor. The processor will be interfaced with a plotter.

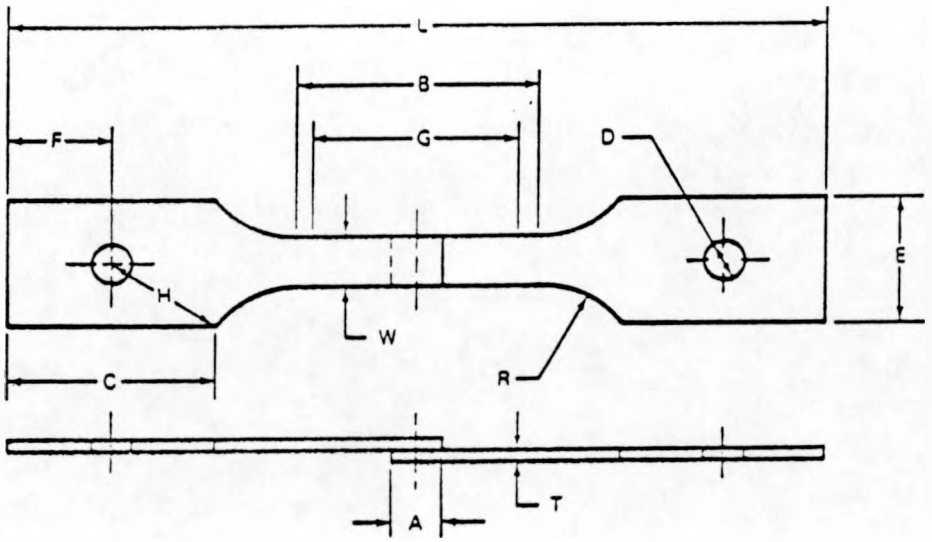

Description - Modified Standard

G - gage length ..... 0.48"
W - width ..... 0.125"
T - thickness ..... 0.027"
R - radius of fillet, min. ..... 0.125"
L - overall length, min. ..... 1.92"
B - length of reduced section, min. ..... 0.54"
C - length of grip section, min.. 0.48"
E - width of grip section approx. 0.30"
D - diameter of hole for pin .... 0.125"
F - edge distance from pin ,approx ..... 0.25"
A - joint overlap ..... 0.28"

Figure 34. AWS Standard Pin Loaded Single-Lap Shear Test Specimen

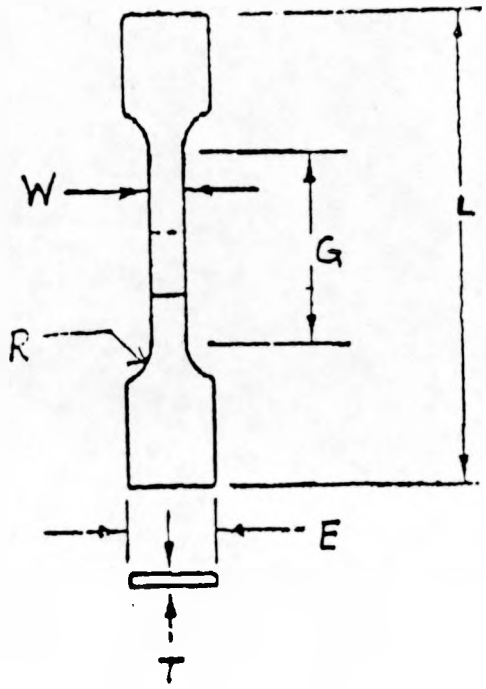

Description - Miniature

G - gage length.....0.201"
W - width.....0.040"
T - thickness.....0.027"
R - radius of fillet, min.....0.063"
L - overall length, min.....0.500"
E - width of grip section approx..0.100"
A - joint overlap.....0.08"-0.11"

Figure 35. Miniature Tensile Specimen Dimensions

III. RECENT RESULTS

Preliminary results of induction brazing of GLIDCOP Al-15 using the BAg-5 alloy have been obtained by varying the heating time and power used. The best brazing results were obtained using a power setting of 45 to 50 for the pin-loaded specimens and a setting of 55 for the miniature samples. The greater power requirements of the miniature samples was the result of fabrication of a large specimen from which the miniatures were machined. The minimum brazing time required to produce mechanically sound joints was 4 to 5 seconds using a 50 Kw induction furnace and a tightly wound oval-shaped helical coil. Both the miniature and the pin loaded specimens required this amount of brazing time. For times less than 4 seconds, the filler metal did not completely melt resulting in incomplete bonding. At brazing time of 6 seconds the base copper alloy had a tendency to distort (wrinkle). The alloy started to melt in 7 to 8 seconds.

Table 12 shows some typical values of yield strength for pin loaded samples along with the overlap length and the furnace power settings. For the pin-loaded specimens with an overlap of slightly over 0.25 inches, the yield strength was generally of the same order as that of the unbrazed material. This would indicated that little degradation of the alloy occurred during induction brazing under the given conditions.

Table 12. Yields strength of induction brazed pin-loaded GLIDCOP Al-15 joints. (Braze time - 4 seconds).

Yield Strength (MPa)	Overlap length (inches)	Power Setting (unitless)
328	.272	55
228	.304	55
313	.270	50
324	.309	50
365	.285	45
316	.265	45
ORNL yield strength data at room temperature for unbrazed GLIDCOP Al-15		
315		
325		
345		

Calculations were performed to study the extent of diffusion of silver from the brazing alloy into the GLIDCOP Al-15 base material. Such calculations could help to determine the possible damage caused by diffusion of silver to both the microstructure and properties of the joint as a result of induction brazing. The following assumptions were made in these calculations.

1. Silver (impurity) diffuses into copper (solvent)
2. Original silver content in Glidcop Al-15 was 0%
3. Diffusion time of 2 seconds
4. Fick's second law with the form of

$$(C_{Ag} - C_x)/(C_{Ag} - C_o) = \text{erf}\ \{X/[2 * \text{square root}(D*t)]\} \quad \ldots\ldots\ldots (1)$$

The following values were used in the above equation:

1. Silver content in the braze filler (BAg-5) was 45%
2. Solvent: copper
   Impurity: silver
   Diffusion coefficient of silver in copper:
   0.63 cm^2/sec [46]
   Activation energy for volume diffusion:
   46.5 Kcal/mole.

Activation energy for surface and grain boundary diffusion was assumed to be one-half of that for volume diffusion: 23.3 Kcal/mole.

The resulting data on the diffusion of silver into copper are listed in Table 13.

Table 13. Amount of silver (C_x in equation 1) diffused into copper as a function temperature and depth of penetration.

Depth of Penetration into copper (in.)	Percentage of Silver Present Temperature 1000°C	900°C	800°C
Volume Diffusion			
0.001	0.0	0.0	0.0
0.0001	5.4	0.0	0.0
Surface and Grain Boundary Diffusion			
0.001	39	36	32
0.0001	45	45	45

Examination of the microstructure of the brazed joints indicated that the brazing procedure produced virtually no diffusion zone at the copper-silver interface (Figure 14). Also, no indication of recrystallization was found in the in the GLIDCOP alloy after brazing. The size of microhardness indentations showed little or no difference along the length of the alloy after brazing or between the alloy and the brazing alloy.

Twelve miniature tensile specimens with brazed joints have been made and six have been tensile tested (Table 14). Miniature samples were made by machining small specimens from a larger overlap joint. Machining was tedious and time consuming. The brazing operation produced inconsistent

samples because the filler metal thickness could not be controlled in the large overlap. The filler metal had a tendency to melt and run with gravity producing a thickness variation. Some of the filler tended to be extruded from the joints and bonded to the Glidcop outside of the overlap. This produced locally thickened sections. This local thickening will be difficult to correct when dealing with specimens of such dimensions. In addition, since the sheet thickness of the Glidcop alloy remains the same, the change in thickness of the filler metal would now be large relative to the width of the joint. These specimens contained varying overlap lengths and joint thicknesses.

The small size of these miniature specimens made fabrication more difficult than for that of the larger specimens. Also, the bending moment due to eccentric loading during tensile testing is more significant with the miniature specimens than with the other samples. This probably resulted in incorrect strain measurements obtained during tensile testing of the six miniature specimen in Table 14. In addition, small imperfections are relatively larger compared to the sample dimensions and all measurements must be made with greater precision.

Table 14. Miniature tensile specimen joint dimensions

Width (inch)	Overlap Thickness (inch)	Overlap Length (inch)	Filler Thickness (inch)	Yield Strength MPa	Tensile Strength MPa	Fracture Relative to Brazed Area
0.037	0.062	0.085	0.008			
0.035	0.053	0.110	0.001			
0.044	0.055	0.105	0.003			
0.043	0.053	0.105	0.001	270	316	outside
0.044	0.060	0.080	0.008			
0.045	0.059	0.080	0.007	192	266	outside but w/cracking in brazed region
0.039	0.053	0.105	0.001	153	198	outside
0.040	0.056	0.080	0.004			
0.0385	0.056	0.100	0.004			
0.0425	0.054	0.095	0.002	260	307	outside
0.040	0.062	0.085	0.002	300	300	inside
0.040	0.063	0.085	0.003	230	288	inside

IV. DISCUSSION

The initial results indicate that a satisfactory induction brazing process using BAg-5 can be achieved. The 4 to 5 seconds brazing cycle provides a sound bond between the filler and the Glidcop alloy without the use of a wetting agent (flux). Additionally, very little oxidation occurred even though neither a flux or a protective atmosphere were used. Minimal secondary cleaning will be required.

The average yield strength of the pin-loaded specimens was 329.2 MPa with an average deviation of 14.3 MPa. (The room temperature average yield strength from ORNL data of unbrazed Glidcop was 325 MPa.) No significant loss in yield strength was incurred during the brazing process. The 228 MPa value was discarded because of premature failure resulting from improper joint fabrication.

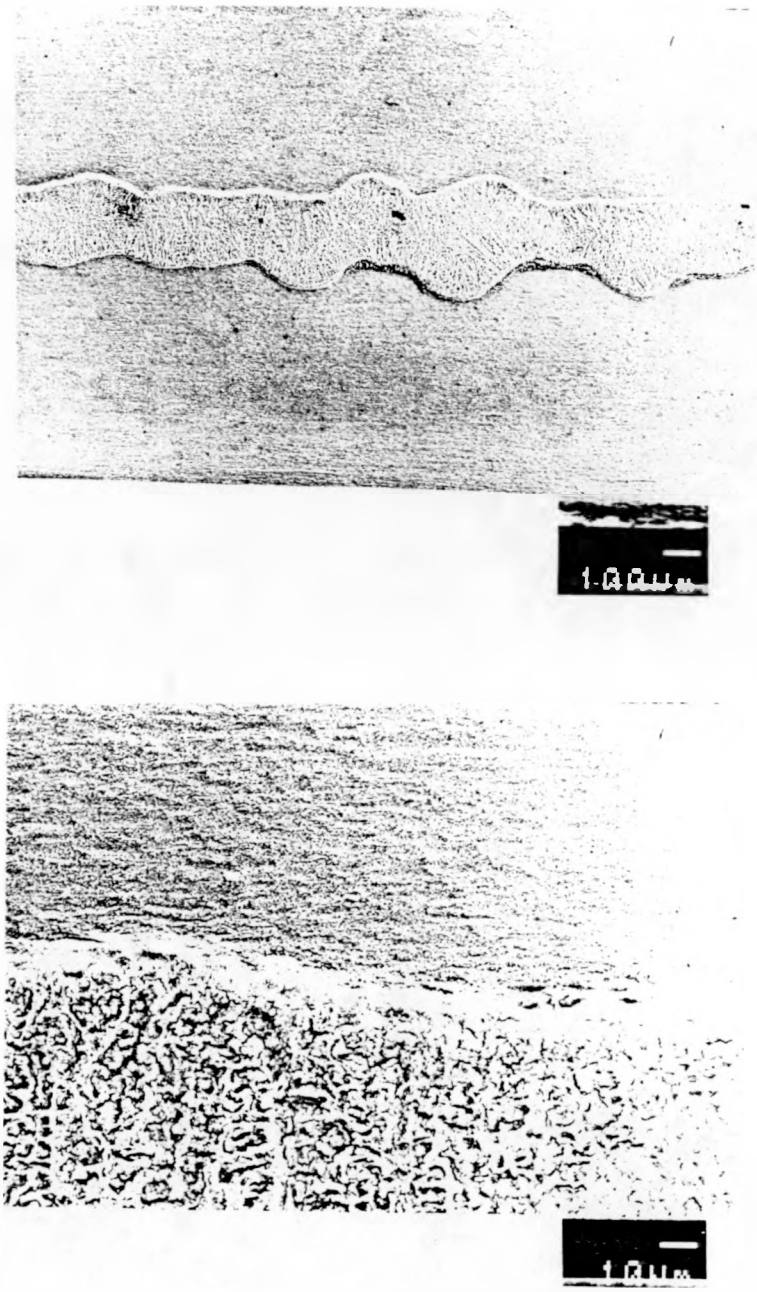

Figure 36. SEM photomicrographs of a pin-loaded brazed joint: (a) Low magnification showing joint at center and (b) higher magnification showing the brazing alloy BAg-5 at the bottom.

BIBLIOGRAPHY

1. D. R. Harries, "Ferritic/Martensitic Steels for use in Near-Term and Commercial Fusion Reactors," Proc. of Topical Conference on Ferritic Alloys for use in Nuclear Energy Technology, TME/AIME, June 19-23, 1983, Snowbird, Utah, pp. 141-155.

2. M. Ma Benjamin, Nuclear Reactor Materials and Applications, Van Nostrand Reinhold Company, New York, 1983.

3. Robert A. Gross, Fusion Energy, John Wiley & Sons, Inc., 1984. pp. 13-15.

4. F. W. Wiffen and R. T. Santoro, "Control of Activation Level to Simplify Waste Management of Fusion Reactor Ferritic Steels Components," ibid. ref.[1], pp. 195-200.

5. J. T. Adrian Roberts, Structural Materials in Nuclear Power Systems, Plenum Press, New York, 1981.

6. Kenneth Evans, Jr. et al., "Wildcat: A Commercial Deuterium-Deuterium Tokamak Reactor," Nuclear Technology/Fusion, Vol. 4, No. 2, Part 1, Sep. 1983, pp.226-236.

7. E. E. Bloom, R. W. Conn, J.W. Davis, R. E. Gold, R. Little, K. R. Schultz, D. L. Smith and F. W. Wiffen, "Low Activation Materials for Fusion Applications," Proc. of the third Topical Meeting on Fusion Reactor Materials, September 19-22, 1983, Albuquerwue, New Mexico, USA, pp. 17-26.

8. R. L. Klueh and W. R. Corwin, "Impact Behavior of Cr-W Steels," Journal of Materials Engineering, Vol. 11, No. 2, 1989, pp. 169-175.

9. H. T. Lin and B. A. Chin, "Properties of Welded Low Activation Ferritic Steels," Fusion Reactor Materials Semiannu. Prog. Rep., Mar. 31, 1987, DOE/ER/0313/2, pp. 135-150, Office of Fusion Energy.

10. American Society for Metals, ASM Metals Handbook, 9th Edition, Vol. 6, Metals Park, OHIO, 1983.

11. K. E. Thelning, Steel and its Heat Treatment, Butterworths, London, 1984.

12. R. W. K. Honeycombe, Steels-Microstructure and Properties, Edward Arnold Ltd. and ASM, Metals Park, OHIO, 1982.

13. W. W. Cias, Phase Transformation Kinetics and Hardenability of Medium-Carbon Alloy Steels, Climax Molybdenum Co., Greenwich, Conn., 1972.

14. George Krauss, Principles of Heat Treatment of Steel, ASM, Metals Park, OHIO, 1980, pp. 43-83.

15. Edgar C. Bain and Harold W. Paxton, Alloying Elements in Steel, ASM, Metals Park, OHIO, 1961.

16. R. L. Klueh and R. W. Swindeman, Mechanical Properties of a Modified 2 1/4 Cr-1Mo Steel for Pressure Vessel Applications, ORNL-5995, Oak Ridge National Laboratory, Oak Ridge, TN, 1983.

17. R. L. Klueh and J. M. Vitek,"The Development of Ferritic Steels for Fast Induced-Radioactivity Decays," pp. 141-146 in ADIP Semiannu. Prog. Rep., Sep. 30, 1984, DOE/ER/0045/13, U. S. DOE, Office of Fusion Energy.

18. K. Yoshikawa, A. Iseda, H. Teranishi, F. Masuyama, T. Daikoku and H. Haneda, "Development of 12Cr-1Mo-1W-V-Nb Steel for Elevated Temperature Applications," High Temperature Alloys-Their Exploitable Potential, Elsevier Applied Science, London, 1987, pp. 247-256.

19. E. J. Vineberg, T. B. Cox, C. C. Clark and P. boussel, "Development of a Duplex Structure 12Cr-1.5Mo-1W Steel for Elevated Temperature Applications," ibid. ref. [18], pp. 287-296.

20. American Society for Metals, ASM Metal Reference Book, ASM, Metals Park, OHIO, 1983, p.437.

21. R. L. Klueh, "The Development of Ferritic Steels for Fast Induced-Radioactivity Decay," ADIP Semiannu. Prog. Rep., Sep. 30, 1985, DOE/ER/0045/15, U. S. DOE, Office of Fusion Energy.

22. Donald R. Askeland, The Science and Engineering of Materials, PWS Engineering ,Boston, Massachusetts, 1984, p.84.

23. J. S. Kirkaldy and D. J. Young, Diffusion in the Condensed State, The Institute of Metals, London, 1985.

24. J Crank, The Mathematics of Diffusion, Oxford University Press, London, 1975.

25. American Society for Metals, ASM Metals Handbook, 9th Edition, Vol. 4, Metals Park, OHIO, 1983.

26. Erwin Kreyszig, Advanced Engineering Mathematics, John Wiley and Sons, New York, 1972.

27. N. M. Ghoniem, J. Blink and N. Hoffman, "Selection of Alloy Steel Type for Fusion Power Applications in the 350°-500°C Temperature Range," ibid. ref. [1], pp.185-193.

28. E. J. Vineberg, T. Wada, T. B. Cox and C. C. Clark, "Weldability of Duplex Structure 12Cr-(Mo,W) Steels," Conference Proceedings on Welding in /energy Related Projects, Welding Institute of Canada, 1984, pp. 235-245.

29. J. F. Hilderbrand, J. R. Foulds and T. A. Lechtenberg, "An Assessment of the Weldability of HT-9 using a Y-Groove Test," ADIP Semiannu. Prog. Rep., Sep. 1983, DOE/ER/0045/11, pp. 152-154, Office of Fusion Energy.

30. D. S. Gelles, F. H. Huang and N. F. Panayotou, "Fractographic Examination of Compact Tension Specimens of Unirradiated HT-9 and Modified 9Cr-1Mo Welds," ADIP Semiannu. Prog. Rep., Mar. 1982, DOE/ER/0045/8, pp.442-459, Office of Fusion Energy.

31. F. H. Huang, "Fracture Toughness of Unirradiated HT-9 and Modified 9Cr-1Mo Welds," ADIP Semiannu. Prog. Rep., Sep. 1982, DOE/ER/0045/9, pp. 221-229, Office of Fusion Energy.

32. Vinod K. Sikka, "Development of Modified 9Cr-1Mo Steel for Elevated-Temperature Service," ibid. ref. [1], pp. 317-327.

33. J. F. King and S. A. David, "Electron Beam Welding of Heavy Section Ferritic Steels," Advances in Welding Science and Technology, S. A. David, ASM, 1986, pp.349-355.

34. R. L. Klueh and E. E. Bloom,"Alloy Development for Fast Induced-Radioactivity Decay for Fusion Reactor Applications," pp. 11-20 in ADIP Semiannu. Prog. Rep., Sep. 20, 1983, DOE/ER/0045/11, U. S. DOE, Office of Fusion Energy.

35. R. L. Klueh, "The Development of Ferritic Steels for Fast Induced-Radioactivity Decay," ADIP Semiannu. Prog. Rep., Mar. 1986, DOE/ER/0045/16, pp. 109-113, Office of Fusion Energy.

36. R. L. Klueh, "The Development of Ferritic Steels for Fast Induced-Radioactivoty Decay," Fusion Reactor Materials Semiannu. Prog. Rep., Mar. 31, 1987, DOE/ER/0313/2, pp. 151-161, Office of Fusion Energy.

37. R. L. Klueh and P. J. Maziasz, "The Development of Ferritic Steels for Fast Induced-Radioactivity Decay," Fusion Reactor Materials Semiannu. Prog. Rep., Sep. 1987, DOE/ER/0313/3, pp. 161-169, Office of Fusion Energy.

38. R. L. Klueh and W. R. Corwin, "Impact Behavior of Cr-W Steels," J. Materials Engineering, Vol. 11, No. 2, 1989, pp.169-175.

39. George E. Dieter, Mechanical Metallurgy, McGraw-Hill Inc., New York, 1976, pp. 348-353.

40. Kenneth Eastering, Introduction to the Physical Metallurgy of Welding, Butterworths Company, London, 1983.

41. W. C. Lesile, The Physical Metallurgy of Steels, McGraw-Hill book company, New York, 1981.

42. B. A. Chin and R. C. Wilcox," The Effect of Heat Treatment on the Impact Properties of a 12Cr-1Mo-V-W Steel," ibid. ref. [1], pp.347-356.

43. K. Anderko, K. David, W. Ohly, M. Schirra, and C. Wassilew, "Optimization Work on Niobium Stabilized 12% CrMoVNb Martensitic Steels for Breeder and Fusion Reactor Applications," ibid. ref. [1], pp.299-306.

44. R. W. K. Honeycombe, Structure and Strength of Alloy Steels, Climax Molybdenum Company, London, 1974.

45. R. L. Klueh, P. J. Maziasz and W. R. Corwin, "Development of Ferritic Steels for Fusion Reactor Applications," ORNL-6472, Oak Ridge National Laboratory, Oak Ridge, TN, 1988.

46. C. Tomizuka, quoted by D. Lazarus, "Solid State Physics," Vol. 10, p. 117, Academic Press, Inc., New York, 1960.